

# Implicit and explicit renormalization: two complementary views of effective interactions

E. Ruiz Arriola<sup>a</sup>, S. Szpigel<sup>b,\*</sup>, V. S. Timóteo<sup>c</sup>

<sup>a</sup>*Departamento de Física Atómica, Molecular y Nuclear and Instituto Carlos I de Física Teórica y Computacional  
Universidad de Granada, E-18071 Granada, Spain*

<sup>b</sup>*Centro de Rádio-Astronomia e Astrofísica Mackenzie, Escola de Engenharia, Universidade Presbiteriana Mackenzie  
01302-907, São Paulo, SP, Brasil*

<sup>c</sup>*Grupo de Óptica e Modelagem Numérica - GOMNI, Faculdade de Tecnologia - FT, Universidade Estadual de Campinas - UNICAMP  
13484-332, Limeira, SP, Brasil*

---

## Abstract

We analyze quantitatively the interplay between explicit and implicit renormalization in Nuclear Physics. By explicit renormalization we mean to integrate out higher energy modes below a given cutoff scale using the similarity renormalization group (SRG) with a block-diagonal evolution generator, which separates the total Hilbert-space into a model space and its complementary. In the implicit renormalization we impose given conditions at low energies for a cutoff theory. In both cases we compare the outcoming effective interactions as functions of the cutoff scale. We carry out a comprehensive analysis of a toy-model which captures the main features of the nucleon-nucleon ( $NN$ )  $S$ -wave interaction at low energies. We find a wide energy region where both approaches overlap. This amounts to a great simplification in the determination of the effective interaction. Actually, the outcoming scales are within the expected ones relevant for the physics of light nuclei.

**Keywords:** Nuclear Force, Renormalization, Similarity Renormalization Group.

---

## 1. Introduction

The idea of renormalization group from a Wilsonian point of view is quite intuitive and appealing [1]. A truncated Hilbert space is considered below some given maximal energy where the relevant physical degrees of freedom are taken into account explicitly. All states above that maximal energy are integrated out and contribute to the structure of operators and their couplings in the reduced Hilbert state via scale-dependent effective interactions. The renormalization group equations arise from the requirement that physical results ought to be independent on the chosen numerical maximal energy value. While one may identify a fundamental underlying theory with the corresponding elementary degrees of freedom, the so-called *ab initio* calculations may not necessarily be the most efficient way to pose the quantum mechanical many-body problem of composite and extended interacting constituent particles. Actually, for a self-bound system its compositeness vs the elementary character depends on the shortest de Broglie wavelength involved in the physical process under consideration as compared to the typical length scales characterizing the interaction among constituents. For *known* interactions the Wilsonian renormalization group approach proves a convenient computational strategy to tackle the many-body problem.

In Nuclear Physics the interaction among nucleons is *unknown* fundamentally and precisely except at long distances where one-pion Exchange (OPE) dominates. At shorter distances the interaction may be constrained from fits to nucleon-nucleon ( $NN$ ) scattering data up to a given maximum energy and with a given accuracy (see Refs. [2–5] for the most recent upgrade in the elastic regime for np and pp data). Thus, the particular status of the nuclear force makes renormalization group methods an ideal tool to address the problem of nuclear binding.

---

\*Corresponding author.

Email address: szpigel@mackenzie.br (S. Szpigel)

In the case of atomic nuclei glued together by the  $NN$  force the most troublesome issue for nuclear structure calculations is the appearance of an inner large core of about  $a_c = 0.5\text{--}0.6$  fm which becomes visible for  $NN$  scattering at pion production threshold [6] (see however Ref. [7] for an alternative interpretation). This distinct feature generates a strong short-range repulsion which complicates enormously the solution of the multinucleon problem limiting the maximal number of nucleons in *ab initio* calculations [8]. On the other hand, because the net effect of the core is to prevent particles to come too close in the nucleus ground-state the net contribution to the binding-energy stemming from distances smaller than the core is tiny. From this point of view one may equally assume weakly interacting particles at short distances, thus under these circumstances the core may be replaced by a suitable soft-core short-distance interaction which keeps invariant the scattering information.

With this perspective in mind, the idea of effective interactions has been developed after the early proposals of Goldstone [9], Moshinsky [10] and Skyrme [11] and Moszkowski and Scott [12] as a way to cut the gordian knot of the Nuclear Many-Body Problem represented by strong short-range repulsion. This allowed to take advantage of the much simpler mean field framework based on those effective interactions [13] (for a review see e.g. [14]). The main problem of the effective interaction approach is both the proliferation of independent parameters as well as their huge numerical diversity (see e.g. the recent compilation of parameters [15]). This reflects both the lack of a unambiguous link to the fundamental two-body interaction as well as the quite disparate finite nuclei and nuclear matter observables which have been used to fix the effective Hamiltonian parameters. An effort has been made [16] (see e.g. Ref. [17] for a similar setup and [18, 19] for alternative views) in order to understand the origin of the two-body effective interactions from free space  $NN$  scattering without invoking finite nuclei nor nuclear matter properties. This point of view corresponds to what will be called here as *implicit* renormalization.

These somewhat intuitive considerations have been made more precise by a novel re-interpretation of the Nuclear Many-Body Problem from the Wilsonian renormalization group point of view. The novel insight, dubbed as  $V_{\text{low } k}$ , is to provide an alternative approach to the determination of effective interactions *directly* from the  $NN$  bare potentials fitted to the scattering data [20–23] (for reviews see e.g. [24–27] and references therein) and their characterization as finite cutoff counterterms [28]. This point of view corresponds to what will be called here as the *explicit* renormalization. The basis of the whole framework has been to recognize the relevance of choosing the proper physical scale resolution in the formulation of the problem. This amounts to a great simplification since at the relevant scales the many-body problem is posed in terms of effective degrees of freedom and hence the interaction decreases and softens. Thus, a mean field solution can be used as a reliable zeroth order approximation, from where corrections can perturbatively be computed. Moreover, when the maximum energy is taken at about pion production threshold or below, the  $V_{\text{low } k}$  interaction does not depend on what particular *bare* potential was used to fit  $NN$  scattering data. This universal character of model independent effective interactions constitutes the main appeal of the approach.

It should be kept in mind that this  $V_{\text{low } k}$  method has not yet been applied to long-range interactions such as Coulomb or van der Waals type <sup>1</sup>. As it is well known, potentials can and have been derived from field theory principles by analyzing the scattering problem in perturbation theory (see e.g. Ref. [31] for a comprehensive exposition). The outgoing meson-exchange potentials correspond to Yukawa-like forms at long distances [32], and hence provide a finite range for the interaction. On the other hand, the same derivations provide singular interactions when directly extrapolated to short distances. In momentum-space these interactions lead to ultraviolet divergencies. The interpretation of these singularities has been intensively analyzed in the literature using field theoretical renormalization group ideas (see e.g. [33] for a discussion within the One-Boson-Exchange picture and references therein). From a practical point of view, these approaches can be thought of as introducing a short-range potential (which acts as a regulator) which is actually fixed by some scattering properties (corresponding to renormalization conditions). In fact, the long-distance behavior turns out to be regulator-independent. In this paper we are not concerned about how a finite-range interaction is deduced from an underlying theory nor which procedure was used to deal with the short-range behavior, and for our purposes we will assume that no serious short-distance singularity is present in the interaction. Rather, we want to analyze the behavior of the system when the scale resolution changes, and more specifically how effective interactions for the Nuclear Many-Body Problem do exhibit the necessary scale-dependence. We point out that the most recent formulation of the problem is via the similarity renormalization group (SRG) method [22, 25, 34], where tremendous simplifications arise which entitle to circumvent the problem at the relevant scales needed for light nuclei.

---

<sup>1</sup>It should be noted that for current state-of-the-art many-body calculations of nuclei the Coulomb contributions are now routinely included in the SRG evolution (see e.g., [29, 30]).

In the present paper we want to analyze the SRG method with a block-diagonal (BD) generator [35] as applied to the two-body problem<sup>2</sup>. This allows to implement, through a continuous and unitary evolution of a system of coupled differential equations, a block-diagonal separation of the Hilbert-space in two orthogonal (decoupled) subspaces  $\mathcal{H} = \mathcal{H}_P \oplus \mathcal{H}_Q$ , which are below or above a given momentum cutoff  $\Lambda$  respectively. The SRG evolution is carried out as function of a momentum-dimension parameter  $\lambda$  referred to as the SRG-cutoff, which runs from  $\lambda = \infty$  (the ultraviolet limit) to  $\lambda = 0$  (the infrared limit) and interpolates between a *bare* Hamiltonian,  $H_{\lambda=\infty}$ , and the block-diagonal one  $H_{\lambda=0}$  in a unitary way  $H_{\lambda=0} = UH_{\lambda=\infty}U^\dagger$ . This is a unitary implementation [35] to all energies of the previously proposed  $V_{\text{low } k}$  approach [20], where the higher-energy states are missing, and in practice a free theory is assumed above the energy determined by the momentum cutoff  $\Lambda$ . For the rest of the paper we will refer to this  $\Lambda$  as the  $V_{\text{low } k}$ -cutoff to be identified with the block-diagonal SRG one. We emphasize that a complete Hilbert-space separation corresponds to the limit  $\lambda \rightarrow 0$ . The SRG method has been applied to the two- [22], three [36] and many-body problem [29, 37–41]. The role of effective and long-distance symmetries has been analyzed only very recently [42–44]. Toy models have also been used to understand relevant features of the equations [45, 46].

As mentioned, the SRG flow-equations are differential equations in the SRG-cutoff  $\lambda$  for unbound operators defined on the Hilbert-space, and they have only been solved exactly for very simple cases [47]. For more realistic cases, one has to resort to numerical analysis; SRG flow-equations are solved on a finite  $N$ -dimensional momentum grid,  $p_n$ , which introduces an infrared resolution scale  $\Delta p_n$  into the problem. Furthermore, an auxiliary numerical cutoff  $P_{\text{max}}$  must also be introduced from the very start, under the assumption that high-momentum states are truly irrelevant and hence decouple. Thus, a finite dimensional Hilbert-space of dimension  $N$  remains. This discretization will be of utmost relevance for our analysis as we discuss briefly below.

The evolution along the SRG trajectory strictly requires the SRG-cutoff  $\lambda$  to be a continuous variable. In practice, however, some integration method is used to numerically solve the SRG flow-equations which requires a further grid in the SRG-cutoff,  $\lambda_i$ . This new discretization introduces an integration step  $\Delta\lambda_i$  which acts as an additional infrared resolution scale and can efficiently be made dependent on the actual  $\lambda_i$  value. Obviously, we must take  $\Delta\lambda_i$  small enough not to jeopardize the unitarity of the SRG transformation, a feature which has to be checked during the course of the evolution<sup>3</sup>. It turns out that evolution steps  $\Delta\lambda_i$  have to become smaller as  $\lambda_i$  approaches the origin. This is partly due to the non-linear character of the SRG flow-equations and the onset of stiffness due to the large dimensionality of the model space. Of course, the existence of two small momentum scales  $\Delta p_n$  and  $\Delta\lambda_i$  suggests some critical slowing down of the calculations. Furthermore, when the  $V_{\text{low } k}$  cutoff  $\Lambda$  (which takes values on the momentum grid  $p_n$ ) is also small,  $\Lambda \leq \Delta p_n$ , we expect some dynamics cross-over as the discretization effects become relevant and hence large deviations from the continuum are expected. Within the finite dimensional reduction of the problem, the meaning of convergence of the SRG evolution as the SRG cutoff  $\lambda$  goes from the  $\lambda = \infty$  to  $\lambda = 0$  is not particularly subtle from a mathematical viewpoint. Technically, the Hamiltonian is defined as an operator on a Hilbert-space. However, the SRG evolution deals with a family of unitarily equivalent operators, and hence one must introduce some metric to measure the distance between operators. As it is well known in finite dimensional spaces all metrics are equivalent. That means that if convergence is accomplished according to a given metric any other metric does also exhibit convergence. In practice one can check individual matrix-elements, for instance. This of course poses the problem of the continuum limit, which to our knowledge has never been discussed in detail within the present context, so some choice of how the limits are taken must be made. In all our numerical implementations of the SRG flow-equations we will assume that the SRG limit is taken first and only then the continuum limit will be pursued.

The basic goal of the BD-SRG (or equivalently  $V_{\text{low } k}$ ) is to choose  $\Lambda$  small enough to filter out model-dependent small-distance physics and make the many-body problem more perturbative, but large enough to keep the relevant and well-constrained low-energy degrees of freedom in the Hilbert space for few- or many-body calculation. In this sense the typical energy scale  $\Lambda$  is set by the pion mass or, equivalently, the energy scale up to where the phase shift analysis can be reliably be performed. Nonetheless, the limit  $\Lambda \rightarrow 0$  is requested to fix the renormalization condition with lowest energy scattering. As we will show, the implicit renormalization handles the continuum limit for small  $\Lambda$ 's, a regime where the finite-grid proves extremely inefficient. On the other hand, when we try to extend this SRG solution

<sup>2</sup>It is noteworthy that this block-diagonal SRG approach could but has not yet been applied to multinucleon problem after properly handling the CM motion.

<sup>3</sup>Algorithms which preserve unitarity exactly, regardless of the evolution step, will be discussed elsewhere.

to higher  $\Lambda$ 's the finite-range aspects of the interaction are lost. We envisage a possibility of reducing the number of grid points precisely when the finite-range becomes relevant.

We consider a simple separable gaussian potential toy-model for the two-body nuclear force inspired by the  $^1S_0$  and  $^3S_1$  partial-wave channels and perform a complete study in the framework of the SRG. These two cases illustrate the situation where either none or just one bound-state (corresponding to the deuteron) are present. The idea is to investigate the infrared limit ( $\lambda \rightarrow 0$ ) of the SRG with the block-diagonal generators which is the unitary version of the  $V_{\text{low } k}$  approach. Our toy-model is constructed so that the main  $S$ -wave two-nucleon observables (the phase-shifts at low-momenta and the deuteron binding-energy) are reasonably described with a short-range interaction and makes the SRG evolution towards the infrared limit much more practical. We compare the effective interactions obtained in the explicit and implicit renormalization approaches and analyze to what extent in terms of the corresponding cutoff scales the  $V_{\text{low } k}$  potential can be implicitly described by low-energy parameters without explicitly solving the SRG flow-equations. Shorter accounts of the present work have already been published [48, 49]. Here we provide more details and further results.

## 2. Implicit renormalization: contact theory with a momentum cutoff

Implicit renormalization is defined by looking for a  $NN$  interaction  $V_\Lambda(p, p')$ , regulated by a sharp or smooth momentum cutoff  $\Lambda$ , which reproduces  $NN$  scattering data up to a given center-of-mass (CM) momentum  $p \leq \Lambda$ . This problem has in fact no unique solution as scattering data above that CM momentum are not specified. This is in spirit the idea behind the  $V_{\text{low } k}$  approach <sup>4</sup>.

### 2.1. Effective range expansion for the $NN$ interaction

Here and in what follows we use units such that  $\hbar = c = M = 1$ , where  $M$  is the nucleon mass. The transition matrix  $T$  for the scattering of two nucleons is given by the partial-wave Lippmann-Schwinger (LS) equation

$$T(p, p'; k^2) = V(p, p') + \frac{2}{\pi} \int_0^\infty dq q^2 \frac{V(p, q)}{k^2 - q^2 + i\epsilon} T(q, p'; k^2), \quad (1)$$

where  $V(p, p')$  is the  $NN$  potential in a given partial-wave. At low energies, the on-shell  $T$ -matrix can be represented by an effective range expansion (ERE)

$$T^{-1}(k, k; k^2) = -[k \cot \delta(k) - i k] = -\left[ -\frac{1}{a_0} + \frac{1}{2} r_e k^2 + v_2 k^4 + \mathcal{O}(k^6) - i k \right], \quad (2)$$

where  $k = \sqrt{E}$  is the on-shell momentum in the CM frame,  $\delta(k)$  is the phase-shift,  $a_0$  is the scattering length,  $r_e$  is the effective range and  $v_2$  is a shape parameter. The experimental values of the ERE parameters  $a_0$  and  $r_e$  for the  $S$ -wave channels are given by

$$\begin{aligned} ^1S_0 \text{ channel : } a_0 &= -23.74 \text{ fm; } r_e = 2.77 \text{ fm}, \\ ^3S_1 \text{ channel : } a_0 &= +5.420 \text{ fm; } r_e = 1.75 \text{ fm}. \end{aligned} \quad (3)$$

In order to avoid a numerical integration on the complex plane, which depends on the contour chosen to perform the sum, we use the LS equation for the partial-wave reactance matrix  $R$  with the principal value prescription,

$$K(p, p'; k^2) = V(p, p') + \frac{2}{\pi} \mathcal{P} \int_0^\infty dq q^2 \frac{V(p, q)}{k^2 - q^2} K(q, p'; k^2), \quad (4)$$

where  $\mathcal{P}$  denotes the principal value. This matrix has the advantage of being real and the relation to the on-shell  $T$ -matrix is given by

$$\frac{1}{K(k, k; k^2)} = \frac{1}{T(k, k; k^2)} - i k. \quad (5)$$

<sup>4</sup>There are of course important differences, as in  $V_{\text{low } k}$  the half-off shell equivalence is also required. This spoils by construction self-adjointness of the potential, and a subsequent transformation to a self-adjoint potential must be carried out.

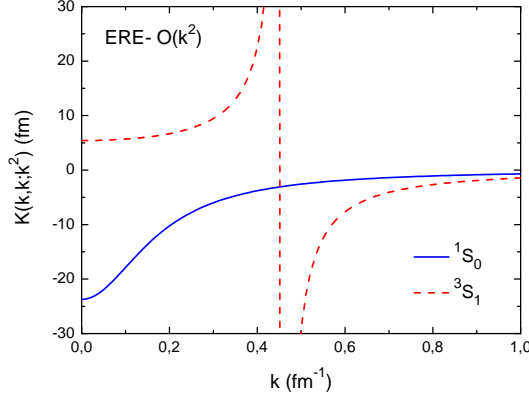


Figure 1: On-shell  $K$ -matrix in the effective range expansion (ERE) to order  $O(k^2)$  for the  $^1S_0$  channel and the  $^3S_1$  channel  $NN$  interactions.

### 2.2. Two-nucleon bound-state

The deuteron bound-state energy  $E_d = -\gamma^2$  can be obtained from the pole of the on-shell  $T$ -matrix for the  $^3S_1$  channel. Using the ERE expansion to order  $O(k^2)$  we have

$$\frac{1}{T(k, k; k^2)} = \frac{1}{a_0} - \frac{1}{2} r_e k^2 + i k = 0 \Rightarrow k = i \gamma = i \left[ \frac{1}{r_e} - \left( \frac{1}{r_e^2} - \frac{2}{a_0 r_e} \right)^{1/2} \right]. \quad (6)$$

One should note that the deuteron pole in the  $T$ -matrix for the  $^3S_1$  channel located at imaginary momentum  $k = i \gamma$  corresponds to a pole in the  $K$ -matrix located at a distinct real momentum  $\beta$ , as shown in Fig. 1. From Eq. (5) we have,

$$\frac{1}{K(k, k; k^2)} = \frac{1}{a_0} - \frac{1}{2} r_e k^2 = 0 \Rightarrow k = \beta = \left[ \frac{2}{a_0 r_e} \right]^{1/2}. \quad (7)$$

The relation between  $\gamma$  and  $\beta$  is then given by

$$\gamma = \left[ \frac{1}{r_e} - \left( \frac{1}{r_e^2} - \beta^2 \right)^{1/2} \right]. \quad (8)$$

By replacing the experimental values of  $a_0$  and  $r_e$  for the  $^3S_1$  channel in Eqs. (6) and (7) we obtain  $\gamma \sim 0.2313 \text{ fm}^{-1}$  and  $\beta \sim 0.4592 \text{ fm}^{-1}$ . Using  $M = 938.919 \text{ MeV} = 4.7581 \text{ fm}^{-1}$  we obtain the deuteron binding energy  $B_d = \gamma^2/M \sim 2.219 \text{ MeV}$ .

### 2.3. Contact theory regulated by a sharp momentum cutoff

While the  $NN$  potential is fairly general, we will analyze here the simple case of hermitian polynomial potentials which correspond to contact or zero-range interactions,

$$\begin{aligned} V(p, p') &= V^{(0)}(p, p') + V^{(2)}(p, p') + V^{(4)}(p, p') + \dots \\ &= C_0 + C_2(p^2 + p'^2) + C_4(p^4 + p'^4) + C'_4 p^2 p'^2 + \dots \end{aligned} \quad (9)$$

In this case the LS equation is divergent, so we can endow the partial-wave  $K$ -matrix regulated by a sharp momentum cutoff  $\Lambda$ ,

$$K_\Lambda(p, p'; k^2) = V(p, p') + \frac{2}{\pi} \mathcal{P} \int_0^\Lambda dq q^2 \frac{V(p, q)}{k^2 - q^2} K_\Lambda(q, p'; k^2). \quad (10)$$

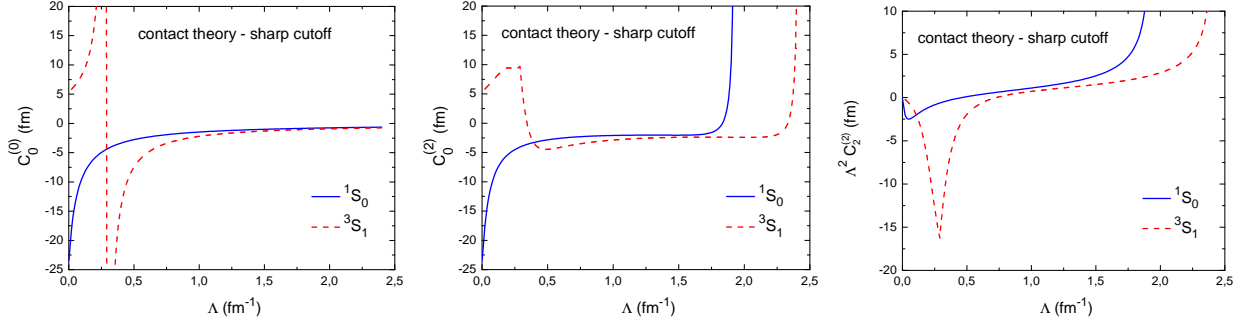


Figure 2: Running of the coefficients  $C_0^{(0)}$ ,  $C_0^{(2)}$  and  $C_2^{(2)}$  with the cutoff  $\Lambda$  for the contact theory in the continuum regulated by a sharp momentum cutoff for the  $^1S_0$  channel and the  $^3S_1$  channel  $NN$  potentials at  $LO$  and  $NLO$ . The coefficients are determined from the analytical solution of the LS equation for the on-shell  $K$ -matrix by fitting the ERE parameters.

and determine the unknown  $\Lambda$ -dependent coefficients  $C_0, C_2, C_4, C'_4, \dots$  through a renormalization procedure. This equation has been solved in a number of occasions and the idea is, for a given cutoff value  $\Lambda$ , to fix the unknown coefficients by fitting the experimental values of the ERE parameters. We solve Eq. (10) analytically and match the expansion of the inverse on-shell  $K$ -matrix in powers of  $k^2$  to the ERE up to a given order.

For the contact theory potential at leading-order ( $LO$ ),

$$V_{LO}(p, p') = V^{(0)}(p, p') = C_0^{(0)}, \quad (11)$$

we obtain

$$\frac{1}{a_0} = \frac{1}{C_0^{(0)}} + \frac{2\Lambda}{\pi}, \quad (12)$$

and for the contact theory potential to next-to-leading-order ( $NLO$ ),

$$V_{NLO}(p, p') = V^{(0)}(p, p') + V^{(2)}(p, p') = C_0^{(2)} + C_2^{(2)} (p^2 + p'^2), \quad (13)$$

a set of two coupled non-linear equations for  $C_0^{(2)}$  and  $C_2^{(2)}$  arise:

$$\frac{1}{a_0} = \frac{45 \pi^2 + 90 C_0^{(2)} \pi \Lambda + 60 C_2^{(2)} \pi \Lambda^3 - 16 C_2^{(2)2} \Lambda^6}{45 C_0^{(2)} \pi^2 - 18 C_2^{(2)2} \pi \Lambda^5}, \quad (14)$$

$$\frac{r_e}{2} = \frac{2 (675 C_0^{(2)2} \pi^2 - 540 C_0^{(2)} C_2^{(2)2} \pi \Lambda^5 + C_2^{(2)} \Lambda (675 \pi^3 + 1125 C_2^{(2)} \pi^2 \Lambda^3 + 600 C_2^{(2)2} \pi \Lambda^6 + 208 C_2^{(2)3} \Lambda^9))}{27 \pi \Lambda (5 C_0^{(2)} \pi - 2 C_2^{(2)2} \Lambda^5)^2}. \quad (15)$$

From the two possible solutions of Eqs. (14) and (15), we choose the one in which  $C_0^{(2)} \rightarrow a_0$  and  $\Lambda^2 C_2^{(2)} \rightarrow 0$  in the limit  $\Lambda \rightarrow 0$ , as shown in Fig. 2. One should note that in the case of the  $^3S_1$  channel the  $LO$  potential coefficient  $C_0^{(0)}$  is singular and the derivatives of the  $NLO$  potential coefficients  $C_0^{(2)}$  and  $C_2^{(2)}$  are discontinuous at  $\Lambda = \pi/2a_0 \sim 0.3 \text{ fm}^{-1}$ , which is the momentum scale where the deuteron bound-state appears. Moreover, as a consequence of Wigner's causality bound, there is a maximum value  $\Lambda_{WB}$  for the cutoff scale  $\Lambda$  above which one cannot fix the potential coefficients  $C_0^{(2)}$  and  $C_2^{(2)}$  by fitting the experimental values of both the scattering length  $a_0$  and the effective range  $r_e$  while keeping the renormalized potential hermitian [50, 51]. Indeed, for  $\Lambda > \Lambda_{WB} \sim 1.9 \text{ fm}^{-1}$  in the case of the  $^1S_0$  channel and  $\Lambda > \Lambda_{WB} \sim 2.4 \text{ fm}^{-1}$  in the case of the  $^3S_1$  channel, the coefficients  $C_0^{(2)}$  and  $C_2^{(2)}$  diverge before taking complex values and hence violating the hermiticity of the effective potential.

We can determine the running of the potential coefficients  $C_0^{(2)}$  and  $C_2^{(2)}$  as a function of the cutoff  $\Lambda$ , but the question is: when do we expect this running to be inaccurate? While the  $NLO$  provides a credible Wigner bound, in

the  $LO$  case there is no reason to stop the evolution. One may of course try to incorporate next-to-next-to-leading-order ( $NNLO$ ) corrections. The problem is that there are two such terms [50]

$$V^{(4)}(p, p') = C_4 (p^4 + p'^4) + C'_4 (p^2 \times p'^2), \quad (16)$$

but there is only *one* low-energy parameter in the ERE at order  $O(k^4)$ , the shape parameter  $v_2$  in Eq. (2). This is so because scattering does not depend just on the on-shell potential. Thus, the implicit renormalization is manifestly not unique beyond  $NLO$ . This is just a manifestation of the existing ambiguities in the inverse scattering problem<sup>5</sup>. The ambiguity is genuine and inherent to the NN interaction; the off-shell part is not uniquely fixed by the scattering data.

Clearly, and even for the coefficients  $C_0^{(2)}$  and  $C_2^{(2)}$ , increasing the  $\Lambda$  values one starts seeing more high-energy details of the theory. In the next section we approach the problem by using a simple toy-model potential which has the main features of the two-nucleon  $S$ -waves, namely no (real) bound-states in the  $^1S_0$  channel and one (real) bound-state in the  $^3S_1$  state (which is identified with the deuteron).

#### 2.4. Contact theory regulated by a smooth momentum cutoff

We aim to compare the effective interactions obtained in the implicit renormalization approach to those obtained in the explicit approach implemented within the framework of the SRG method. Since the SRG flow-equations have to be solved numerically on a finite momentum grid, in order to perform a consistent comparison we consider the implicit renormalization of a contact theory potential regulated by a smooth momentum cutoff on the same grid. The LS equation for the partial-wave  $K$ -matrix with a smooth momentum cutoff is given by

$$K_\Lambda(p, p'; k^2) = V_\Lambda(p, p') + \frac{2}{\pi} \mathcal{P} \int_0^\infty dq q^2 \frac{V_\Lambda(p, q)}{k^2 - q^2} K_\Lambda(q, p'; k^2), \quad (17)$$

where  $V_\Lambda(p, p')$  is the contact theory potential given in Eq. (9) regulated by an exponential function  $f_\Lambda(p) = \exp[-(p/\Lambda)^{2n}]$

$$V_\Lambda(p, p') \equiv \exp[-(p/\Lambda)^{2n}] V(p, p') \exp[-(p'/\Lambda)^{2n}], \quad (18)$$

and  $n = 1, 2, \dots$  determines the sharpness of the regulating function  $f_\Lambda(p)$ .

In the case of a finite momentum grid, the contact theory potential coefficients  $C_i^{(j)}$  are determined from the numerical solution of the LS equation for the  $K$ -matrix by fitting the experimental values of the ERE parameters. Following the method described by Steele and Furnstahl [52], we solve Eq. (17) on a gaussian grid with  $N$  momentum points in the range  $[0, P_{\max}]$  and fit the difference between the corresponding inverse on-shell  $K_\Lambda$ -matrix and the inverse on-shell  $K_{\text{ERE}}$ -matrix to an interpolating polynomial in  $k^2/\Lambda^2$  to highest possible degree for a spread of very small on-shell momenta  $k_{\text{low}} \leq 0.1 \text{ fm}^{-1}$ :

$$\Delta\left(\frac{1}{K}\right) = \frac{1}{K_\Lambda(k, k; k^2)} - \frac{1}{K_{\text{ERE}}(k, k; k^2)} = A_0 + A_2 \frac{k^2}{\Lambda^2} + \dots \quad (19)$$

Then we minimize the coefficients  $A_i$  with respect to the variations of the coefficients  $C_i^{(j)}$ .

In Fig. 3 we compare the running of the coefficients  $C_i^{(j)}$  with the cutoff  $\Lambda$  for the  $LO$  and  $NLO$  contact theory potentials on a finite momentum grid using regulating functions with sharpness parameter  $n = 2, 4, 8$  and  $16$  for different grid sizes  $(P_{\max}; N)$ . As one can observe, when the sharpness parameter  $n$  or the grid size increases we obtain a better agreement with the results for the contact theory in the continuum regulated by a sharp cutoff.

In Fig. 4 we show the on-shell  $K$ -matrix for the  $^1S_0$  channel and the  $^3S_1$  channel  $NN$  potentials at  $NLO$  as a function of the momentum  $k$  for several values of the cutoff scale  $\Lambda$ , both in the contact theory with a sharp cutoff and in the contact theory with a smooth cutoff. As one can observe, in both cases the on-shell  $K$ -matrix changes with  $\Lambda$ , approaching the on-shell  $K$ -matrix in the ERE to order  $O(k^2)$  as  $\Lambda$  increases. One should also note that for the  $^3S_1$  channel the pole is shifted to the left as  $\Lambda$  decreases and vanishes when  $\Lambda < 0.3 \text{ fm}^{-1}$ , which is the threshold scale below which we do not observe a bound-state in the  $^3S_1$  channel.

<sup>5</sup>Actually, from a dimensional point of view the two-body operators with four derivatives are suppressed as compared to contact three-body operators. The off-shellness of the two-body problem can equivalently be translated into some three-body properties.

### 3. Explicit renormalization

#### 3.1. The toy-model: separable gaussian potential

In the applications of the SRG method to Nuclear Physics, realistic potentials which fit  $NN$  data up to the pion-production threshold ( $\sqrt{m_\pi M_N} \sim 400$  MeV) are usually taken as the initial  $NN$  bare interaction. Due to the short-range repulsive core such potentials exhibit a long high-momentum tail, requiring the use of a large value for the auxiliary momentum cutoff  $P_{\max}$  which complicates the numerical convergence when solving the SRG flow-equations<sup>6</sup>. For illustration purposes, in this work we consider as the  $NN$  bare interaction a simple separable gaussian potential toy-model for the  $S$ -waves, given by

$$V(p, p') = C g_L(p) g_L(p'), \quad (20)$$

with a gaussian form factor  $g_L(p) = e^{-p^2/L^2}$ . The potential parameters  $(C, L)$  are determined by fitting the experimental values of the ERE parameters,  $a_0$  and  $r_e$ . For the toy-model potential in the continuum we obtain  $C_{N=\infty}^{1S_0} = -1.915884$  fm and  $(1/L^2)_{N=\infty}^{1S_0} = 0.691269$  fm<sup>2</sup> for the  $1S_0$  channel and  $C_{N=\infty}^{3S_1} = -2.300641$  fm and  $(1/L^2)_{N=\infty}^{3S_1} = 0.415154$  fm<sup>2</sup> for the  $3S_1$  channel.

In the case of a separable potential, it is straightforward to determine the phase-shifts using the *ansatz* for the  $T$ -matrix given by

$$T(p, p'; k^2) = g_L(p) t(k) g_L(p'), \quad (21)$$

where  $t(k)$  is called the reduced on-shell  $T$ -matrix. This leads to the relation

$$k \cot \delta(k) = -\frac{1}{V(k, k)} \left[ 1 - \frac{2}{\pi} \mathcal{P} \int_0^\infty dq q^2 \frac{1}{k^2 - q^2} V(q, q) \right]. \quad (22)$$

As shown in Fig. 5, the  $1S_0$  and  $3S_1$  phase-shifts computed from Eq. (22) for the toy-model potential qualitatively resemble the results from the much used 1993 Nijmegen partial-wave analysis (PWA) [54] or the more recent 2013 upgrades [2–5]. Moreover, the on-shell  $T$ -matrix for the  $3S_1$  channel toy-model potential has a pole located at  $k = i 0.2314$  fm<sup>-1</sup>, corresponding to a satisfactory deuteron binding-energy  $B_d = 2.22$  MeV. The deuteron wave function is obtained as

$$\psi_d(p) = \frac{1}{\sqrt{N}} \frac{g_L(p)}{p^2 + \gamma^2}. \quad (23)$$

The normalization condition,

$$\frac{2}{\pi} \int_0^\infty dp p^2 |\psi_d(p)|^2 = 1, \quad (24)$$

implies that  $\frac{1}{\sqrt{N}} = 0.8548$  fm<sup>1/2</sup>. The matter radius is defined as

$$\frac{1}{2\pi} \int_0^\infty dp |\psi_d(p)|^2 = r_m^2, \quad (25)$$

which gives  $r_m = 1.938$  fm.

#### 3.2. SRG evolution of the toy-model potential

The SRG, developed by Glazek and Wilson [55, 56] and independently by Wegner [57] (for a review see e.g. [58]), is a renormalization method based on a series of continuous unitary transformations that evolve hamiltonians with a cutoff on energy differences. Here we employ the formulation for the SRG developed by Wegner, which is based on a

---

<sup>6</sup>For the Argonne v18 [6] and the Nijmegen II [53] realistic potentials, for example, one needs  $P_{\max} \sim 30$  fm<sup>-1</sup> in order to ensure that the potential matrix-elements have vanished.



non-perturbative flow-equation that governs the unitary evolution of a hamiltonian  $H = T_{\text{rel}} + V$  with a flow parameter  $s$  that ranges from zero to infinity,

$$\frac{dH_s}{ds} = [\eta_s, H_s], \quad (26)$$

where  $\eta_s = [G_s, H_s]$  is an anti-hermitian operator that generates the unitary transformations. The flow parameter  $s$  has dimensions of  $[\text{energy}]^{-2}$  and in terms of a similarity cutoff  $\lambda$  with dimension of momentum is given by the relation  $s = \lambda^{-4}$ . The operator  $G_s$  defines the anti-hermitian generator  $\eta_s$  and so specifies the flow of the hamiltonian. The flow equation is to be solved with the boundary condition  $H_s|_{s \rightarrow 0} \equiv H_0$ , where  $H_0$  ( $\equiv H_{\lambda=\infty}$ ) is the hamiltonian corresponding to the initial *bare* interaction.

Assuming that  $T_{\text{rel}}$  is independent of  $s$ , we obtain

$$\frac{dV_s}{ds} = [\eta_s, H_s]. \quad (27)$$

We take the block-diagonal SRG generator [35] given by

$$G_s = H_s^{\text{BD}} \equiv \begin{pmatrix} PH_sP & 0 \\ 0 & QH_sQ \end{pmatrix}, \quad (28)$$

where  $P$  and  $Q = 1 - P$  are projection operators. In a partial-wave relative momentum-space basis, the projection operators are determined in terms of a momentum cutoff scale  $\Lambda$  that divides the momentum space into a low-momentum  $P$ -space ( $p < \Lambda$ ) and a high-momentum  $Q$ -space ( $p > \Lambda$ ). Here we define the projection operators just as step functions,

$$P \equiv \theta(\Lambda - p); \quad Q \equiv \theta(p - \Lambda). \quad (29)$$

The full hamiltonian  $H_s$  can be written as,

$$H_s \equiv \begin{pmatrix} PH_sP & PH_sQ \\ QH_sP & QH_sQ \end{pmatrix}. \quad (30)$$

The anti-hermitian operator  $\eta_s$  is then given by

$$\eta_s = [G_s, H_s] = \begin{pmatrix} 0 & P\eta_sQ \\ Q\eta_sP & 0 \end{pmatrix}, \quad (31)$$

where

$$P\eta_sQ = PH_sPH_sQ - PH_sQH_sQ \quad (32)$$

$$Q\eta_sP = QH_sQH_sP - QH_sPH_sP. \quad (33)$$

Thus, the SRG flow-equation with the block-diagonal generator can be written in matrix-form as

$$\begin{pmatrix} \frac{d}{ds}[PV_sP] & \frac{d}{ds}[PV_sQ] \\ \frac{d}{ds}[QV_sP] & \frac{d}{ds}[QV_sQ] \end{pmatrix} = \begin{pmatrix} P\eta_sQH_sP - PH_sQ\eta_sP & P\eta_sQH_sQ - PH_sP\eta_sQ \\ Q\eta_sPH_sP - QH_sQ\eta_sP & Q\eta_sPH_sQ - QH_sP\eta_sQ \end{pmatrix}. \quad (34)$$

The potential  $V_s$  can be written as,

$$V_s \equiv \begin{pmatrix} PV_sP & PV_sQ \\ QV_sP & QV_sQ \end{pmatrix}. \quad (35)$$

By choosing the block-diagonal generator, the matrix-elements inside the off-diagonal blocks  $PV_sQ$  and  $QV_sP$  are suppressed as the flow parameter  $s$  increases (or as the similarity cutoff  $\lambda$  decreases), such that the hamiltonian is driven to a block-diagonal form. In the limit  $\lambda \rightarrow 0$  the  $P$ -space and the  $Q$ -space become completely decoupled,

$$\lim_{\lambda \rightarrow 0} V_\lambda = PV_{\text{low } k}P + QV_{\text{high } k}Q = \begin{pmatrix} V_{\text{low } k} & 0 \\ 0 & V_{\text{high } k} \end{pmatrix} \quad (36)$$

Thus, while unitarity implies  $\delta_\lambda(p) = \delta(p)$  for any  $\lambda$  one has

$$\lim_{\lambda \rightarrow 0} \delta_\lambda(p) = \delta_{\text{low } k}(p) + \delta_{\text{high } k}(p) \quad (37)$$

where  $\delta_{\text{low } k}(p) = \delta(p)\theta(\Lambda - p)$  and  $\delta_{\text{high } k}(p) = \delta(p)\theta(p - \Lambda)$  are the phase-shifts of the  $V_{\text{low } k}$  and  $V_{\text{high } k}$  potentials respectively.

Here, we consider the SRG evolution of the toy-model separable gaussian potential described in section 3.1. The parameters  $(C, L)$  are determined from the numerical solution of the LS equation for the  $K$ -matrix by fitting the experimental values of the ERE parameters,  $a_0$  and  $r_e$ . For a gaussian grid with  $N = 50$  momentum points and  $P_{\text{max}} = 5 \text{ fm}^{-1}$  we obtain  $C_{N=50}^{1S_0} = -2.069625 \text{ fm}$  and  $(1/L^2)_{N=50}^{1S_0} = 0.818149 \text{ fm}^2$  for the  $1S_0$  channel and  $C_{N=50}^{3S_1} = -2.952983 \text{ fm}$  and  $(1/L^2)_{N=50}^{3S_1} = 0.581541 \text{ fm}^2$  for the  $3S_1$  channel. One should note that these values are slightly different from those obtained for the toy-model potential in the continuum ( $N = \infty$ ) with the same values of  $a_0$  and  $r_e$ . We solve Eq.(34) numerically, obtaining an exact (non-perturbative) solution for the SRG-evolved toy-model potential (apart from numerical errors). The discretization of the relative momentum space on a grid with  $N$  points leads to a system of  $4N^2$  non-linear first-order coupled differential equations which is solved by using a variable-step fifth-order Runge-Kutta algorithm. In Figs. 6 and 7 we show the SRG evolution of the  $1S_0$  channel and the  $3S_1$  channel toy-model potentials. As one can observe, the diagonal matrix-elements inside the  $P$ -space ( $p < \Lambda$ ) change significantly as the SRG cutoff  $\lambda$  decreases. Such a change becomes smaller as the block-diagonal cutoff  $\Lambda$  increases. On the other hand, the diagonal matrix-elements inside the  $Q$ -space ( $p > \Lambda$ ) remain practically unchanged (apart from a small change for momenta  $p$  near  $\Lambda$ ). The evolution of the fully off-diagonal matrix-elements inside the  $P$ -space is similar. As expected, the fully off-diagonal matrix-elements inside the  $PV_sQ$  block (and the  $QV_sP$  block) go to zero as the similarity cutoff  $\lambda$  decreases. One should also note that in the case of the  $3S_1$  channel potential, the evolution follows a different pattern for  $\Lambda \leq 0.3 \text{ fm}^{-1}$ , which is the scale where the deuteron bound-state appears.

In Fig. 8, we show the on-shell  $K$ -matrices for the  $1S_0$  channel and the  $3S_1$  channel toy-model potentials in the continuum and on a gaussian grid with  $N = 50$  momentum points and  $P_{\text{max}} = 5 \text{ fm}^{-1}$ , compared with the corresponding on-shell  $K$ -matrices obtained from the ERE to order  $\mathcal{O}(k^2)$ . We have checked through explicit calculations that the on-shell  $K$ -matrices for the SRG-evolved toy-model potentials remain invariant under the change of both the similarity cutoff  $\lambda$  and the block-diagonal cutoff  $\Lambda$ , as expected from the unitarity of the SRG transformation.

In order to test the decoupling between the  $P$ -space and the  $Q$ -space in the SRG evolution with a block-diagonal generator, we compute the on-shell  $K$ -matrices for the  $1S_0$  channel and the  $3S_1$  channel SRG-evolved toy-model potentials cut at the block-diagonal cutoff  $\Lambda$ , i. e. with the matrix-elements set to zero for momenta above  $\Lambda$ . As one can observe in Figs. 9, for a given  $\Lambda$  the decoupling improves as  $\lambda$  decreases. For  $\lambda < \Lambda$ , the results are nearly indistinguishable from those obtained with the initial ( $\lambda \rightarrow \infty$ ) potential for momenta  $k < \Lambda$ , except near the deuteron pole (that vanishes for  $\Lambda < 0.3 \text{ fm}^{-1}$ ) in the case of the  $3S_1$  channel potential. One should also note that the position of the deuteron pole changes as the potential evolves and in the limit  $\lambda \rightarrow 0$  approaches that for the initial potential as  $\Lambda$  increases, similar to what happens for the contact theory potential regulated by a sharp or smooth cutoff. In the left panel of Fig. 10 we show the results for the deuteron binding-energy as a function of the cutoff scale  $\Lambda$  evaluated from the numerical solution of Schrödinger's equation with the  $3S_1$  channel potential at  $NLO$  for the contact theory in the continuum with a sharp cutoff and for the contact theory on a gaussian grid with a smooth cutoff (with  $N = 50$  momentum points,  $P_{\text{max}} = 5 \text{ fm}^{-1}$  and  $n = 16$ ). As one can observe, in both cases the deuteron bound-state appears at  $\Lambda \sim 0.3 \text{ fm}^{-1}$ . For the contact theory in the continuum with a sharp cutoff the binding-energy approaches the value obtained from the ERE to order  $\mathcal{O}(k^2)$  as  $\Lambda$  increases. In the case the contact theory on a grid with a smooth cutoff the binding-energy approaches the value obtained for the toy-model potential. One should note that the results obtained for the toy-model potential evolved through the SRG transformation with the block-diagonal generator remain invariant

under the change of both the SRG cutoff  $\lambda$  and the block-diagonal cutoff  $\Lambda$ . In the right panel Fig. 10 we show the results for the deuteron binding-energy as a function of the block-diagonal cutoff  $\Lambda$  evaluated from the numerical solution of Schrödinger's equation with the  $^3S_1$  channel SRG-evolved toy-model potential cut at  $\Lambda$  (i. e. with the matrix-elements set to zero for momenta above  $\Lambda$ ). As a consequence of the decoupling between the  $P$ -space and the  $Q$ -space, for a given  $\Lambda$  ( $> 0.3 \text{ fm}^{-1}$ ) the binding-energy obtained for the cut SRG-evolved potential approaches the value obtained for the initial ( $\lambda \rightarrow \infty$ ) potential provided  $\lambda \ll \Lambda$ <sup>7</sup>.

#### 4. Fitting the explicitly renormalized potential with the contact interactions from the implicit method

We want to compare the running of the coefficients  $C_0^{(2)}$  and  $C_2^{(2)}$  with the cutoff  $\Lambda$  in the contact theory potential at  $NLO$  to the running of the corresponding coefficients  $\tilde{C}_0^{(2)}$  and  $\tilde{C}_2^{(2)}$  with the  $V_{\text{low } k}$  cutoff ( $\equiv \Lambda$ ) extracted from a polynomial fit of the block-diagonal SRG-evolved toy-model potential,

$$V_{\Lambda, \Lambda}(p, p') = \tilde{C}_0^{(2)} + \tilde{C}_2^{(2)} (p^2 + p'^2) + \dots \quad (38)$$

The parameters  $(C, L)$  in the initial ( $\lambda \rightarrow \infty$ ) toy-model potential, given by Eq. (20), and the coefficients  $C_0^{(2)}$  and  $C_2^{(2)}$  in the contact theory potential at  $NLO$  are determined from the numerical solution of the  $LS$  equation for the  $K$ -matrix by fitting the experimental values of the scattering length  $a_0$  and the effective range  $r_e$ . The coefficients  $\tilde{C}_0^{(2)}$  and  $\tilde{C}_2^{(2)}$  are determined by fitting the diagonal matrix-elements of the block-diagonal SRG-evolved toy-model potential for the lowest momenta with the polynomial form.

In Figs. 11 to 14 we show the results for  $\tilde{C}_0^{(2)}$  and  $\Lambda^2 \tilde{C}_2^{(2)}$  extracted from the  $^1S_0$  channel and the  $^3S_1$  channel SRG-evolved toy-model potentials on a gaussian grid (with  $N = 50$  momentum points and  $P_{\text{max}} = 5 \text{ fm}^{-1}$ ), compared to  $C_0^{(2)}$  and  $\Lambda^2 C_2^{(2)}$  obtained for the contact theory potentials at  $NLO$  (on the same grid) regulated by a smooth exponential momentum cutoff with sharpness parameter  $n = 16$ . As one can see, for a given cutoff  $\Lambda$  the coefficients  $\tilde{C}_0^{(2)}$  and  $\Lambda^2 \tilde{C}_2^{(2)}$  extracted from the SRG-evolved toy-model potentials approach the coefficients  $C_0^{(2)}$  and  $\Lambda^2 C_2^{(2)}$  obtained for the contact theory potentials as the SRG cutoff  $\lambda$  decreases. In general, the running of the coefficients becomes more significant as  $\lambda$  approaches  $\Lambda$  and nearly saturates when  $\lambda \leq \Lambda$ . In the case of the  $^1S_0$  channel, the running of  $\Lambda^2 \tilde{C}_2^{(2)}$  deviates from such a pattern for  $\Lambda \leq 0.2 \text{ fm}^{-1}$ . As shown in Fig. 12, the coefficient  $\Lambda^2 \tilde{C}_2^{(2)}$  for the contact theory potential has a dip in this region. In the case of the  $^3S_1$  channel, we observe large discrepancies in the running of both  $\tilde{C}_0^{(2)}$  and  $\Lambda^2 \tilde{C}_2^{(2)}$  for  $\Lambda$  in the range from  $\sim 0.3$  to  $\sim 0.5 \text{ fm}^{-1}$ , even for small values of  $\lambda$ . As shown in Fig. 14, this is the region where the running of the coefficients becomes more significant, which corresponds to the range from the scale where the deuteron bound-state appears to the momenta around the pole in the  $K$ -matrix. Nevertheless, one can see that in the limit  $\lambda \rightarrow 0$  there is a remarkably good agreement between the coefficients extracted from the block-diagonal SRG-evolved toy-model potentials and those obtained for the contact theory potentials.

It is important to point out that the agreement between the running of the coefficients  $C_0^{(2)}$  and  $C_2^{(2)}$  in the contact theory potential and the running of the coefficients  $\tilde{C}_0^{(2)}$  and  $\tilde{C}_2^{(2)}$  extracted from the block-diagonal SRG-evolved toy-model potential as the SRG cutoff  $\lambda$  decreases below  $\Lambda$  can be traced to the decoupling between the  $P$ -space and the  $Q$ -space, which follows a similar pattern. Thus, in the limit  $\lambda \rightarrow 0$  we expect to achieve a high degree of agreement for cutoffs  $\Lambda$  up to  $\Lambda_{\text{WB}}$  determined by the Wigner bound for the contact theory potential.

We could also analyze the constants  $C_4$  and  $C'_4$  appearing in Eq. (9). As already mentioned, these constants (unlike  $C_0$  and  $C_2$ ) feature specific properties of the bare potential, and their running cannot be determined from two-body scattering data alone. This ambiguity was manifest in the implicit method when looking at  $\Lambda \rightarrow 0$ , but the explicit form of the BD-SRG does not solve it; it is hidden in the initial condition at  $\Lambda \rightarrow \infty$ . While it is true that for a given bare NN interaction the explicit method yields a unique answer, the bare interaction itself is not uniquely fixed by the scattering data, as the off-shell part of the interaction cannot be fixed this way. The implicit method just reflects this fact, and it would be misleading to take this feature as a genuine disadvantage of the method. Actually, it is the opposite, the explicit method just inherits the arbitrariness of the original bare two body interaction. Of course, this

<sup>7</sup>Similar plots to Fig. 10 have been particularly inspiring in our recent analysis of the infrared fixed points of the connection between SRG and Levinson's theorem [59].

can only be solved unambiguously by solving implicitly the three- and higher body problem, using the BD-SRG for the CM Hamiltonian, by imposing binding energies and scattering data as renormalization conditions. While this is a possible scheme, it is numerically cumbersome and is left for future research.<sup>8</sup>

## 5. Summary and Outlook

In the present work we have made a thorough investigation on the renormalization of effective interactions for the nuclear force. The main purpose was to display the complementary views between implicit and explicit renormalization. For simplicity, we have focused on the two-nucleon problem and the  $^1S_0$  and  $^3S_1$  states where the interaction is non-perturbative and has either none or one bound-state (the deuteron). To further simplify the analysis, we have considered a separable gaussian potential toy-model as a bare interaction in order to reduce the computational effort. Already at this level, this much assumed complementarity is difficult to test at the desired accuracy.

In the explicit renormalization approach implemented via the SRG method with a block-diagonal generator, the original Hilbert space is separated in two orthogonal sectors according to a given energy boundary. For the case of two-body interactions in a given partial-wave channel this energy can be transformed into a CM momentum cutoff  $\Lambda$ , which corresponds to the analogous  $V_{\text{low } k}$  cutoff. This is carried out by a suitable unitary transformation which can steadily be constructed by using a uniparametric group family via a differential equation in operator space in the SRG cutoff parameter  $\lambda$ . One problem is that the numerical resolution of these differential equations in operator space requires reducing the Hilbert space to a finite number of dimensions,  $N$ , which makes the non-linear system of order  $N^2$ . This introduces a minimum momentum resolution  $\Delta p \sim P_{\text{max}}/N$ . Generally, as  $\lambda \rightarrow 0$  the equations become stiff and thus convergence issues prevent an accurate solution. In practice, when  $\lambda \ll \Delta p$  the differential equations yield numerical spurious results. Thus, in practice the finite  $\Delta p$  prevents an accurate block-diagonalization for  $\Lambda \leq \Delta p$ .

The implicit renormalization approach determines the potential in the low-momentum region in a model independent way by fixing scattering information, and more specifically the scattering length and the effective range. Going beyond these two low-energy parameters or determining the effective interaction to higher energies depends on the details of the bare interaction. Moreover, the equations can be solved analytically in the continuum without any finite momentum grid. This actually allows to work precisely when the explicit renormalization approach does not. Actually, we find that the complementarity of both explicit and implicit approaches is verified in a wide cut-off range  $\Lambda$ . For the  $^1S_0$  and  $^3S_1$  neutron-proton scattering states this range is within  $0.5 \text{ fm}^{-1} \leq \Lambda \leq 1.5 \text{ fm}^{-1}$ . This is a welcome feature, since it suggests that the bulk of the effective interaction operating in finite nuclei can be directly extracted from low-energy  $NN$  data, providing a short-cut to large-scale calculations.

While the complementarity of both explicit and implicit views of the renormalization procedure is taken for granted at *sufficiently* low energies, it is fair to say that within the present context of nuclear interactions it has seldomly been verified to the degree analyzed in the present work and the relevant scales have never been clearly quantified. This requires to pin down the numerical uncertainties with sufficient accuracy in the explicit method. This of course suggests that the implicit renormalization approach may be a better method to determine the effective interaction. This was the purpose of a previous analysis [16] where the Skyrme force parameters just deducible from the  $NN$  interaction were determined until a low-energy saturation was observed. The present discussion provides an *a posteriori* explanation of this observation.

Perturbative discussions provide the customary example to motivate the idea of an effective field theory (EFT). Actually, such a perturbative approach holds true when there are large energy gaps in the theory, since large mass splittings allow for a perturbative treatment due to well known decoupling theorems. Moreover, the existence of energy gaps allows for generous variations of the *a priori* cutoff scale. A prominent example is  $\pi\pi$  scattering at CM energies much smaller than the vector meson masses. In Nuclear Physics, there is no obvious *a priori* energy gap. In the meson exchange picture, multipion exchanges take place before heavier mesons enter the game. This is a good reason why the discussion on the Wilsonian aspects of renormalization becomes considerably more complicated. Given the relatively low scales where the effective interaction strength is saturated, our findings suggest also to critically review

---

<sup>8</sup> One possible strategy is to obtain the constants directly from a reference K-matrix at low energies, which can be obtained from a phenomenological potential. In principle, it is possible to extend the implicit renormalization approach to current high precision forces but the equations cannot be solved as easily (see e.g. Ref. [16] for a complete NLO calculation).

the quantitative role of explicit pions and more specifically the relevance of chiral two-pion exchange (TPE) in the study of the structure of light nuclei. This issue was partially addressed in our previous work [48] and will be discussed comprehensively in an upcoming publication.

While to achieve exact decoupling one has to evolve from  $\lambda = \infty$  to  $\lambda = 0$  it is not obvious from the start which value of  $\Lambda$  defining the model space is optimal. Naively it should be defined by  $\min_{\Lambda} \|QH(0)Q\|$ , whence an insensitivity region around this value should take place. The existence of such a scale is not obvious, but it has been known since many years by the work of Moszkowski and Scott [12] as already recognized by Brown and Holt [60]. The smallest value of the high-momentum  $Q$ -space block-diagonal Hamiltonian is obtained when  $QHQ = 0$ . This corresponds to a situation where above a certain CM momentum scale nucleons behave to a large extent as free particles.

One of the advantages of the implicit renormalization method is that it may be applied in situations where the block-diagonal SRG method cannot due to long tails which intertwine all momentum scales and make a direct numerical solution out of reach. An interesting case corresponds to the van der Waals interactions between neutral atoms [61] where similar trends are found, but the block-diagonal SRG explicit solutions are extremely difficult to obtain.

## Acknowledgements

E.R.A. would like to thank the Spanish DGI (Grant FIS2011-24149) and Junta de Andalucia (Grant FQM225). S.S. is partially supported by FAPESP and V.S.T. thanks FAEPEX (Grant 1165/2014), FAPESP (Grant 2014/04975-9), CNPq (Grant 310980/2012-7) for financial support.

## References

## References

- [1] K. Wilson, J. B. Kogut, The Renormalization group and the epsilon expansion, *Phys.Rept.* 12 (1974) 75–200. doi:10.1016/0370-1573(74)90023-4.
- [2] R. Navarro Perez, J. Amaro, E. Ruiz Arriola, Partial Wave Analysis of Nucleon-Nucleon Scattering below pion production threshold, *Phys.Rev. C* 88 (6) (2013) 024002. arXiv:1304.0895, doi:10.1103/PhysRevC.88.024002, 10.1103/PhysRevC.88.069902.
- [3] R. Navarro Perez, J. Amaro, E. Ruiz Arriola, Coarse-grained potential analysis of neutron-proton and proton-proton scattering below the pion production threshold, *Phys.Rev. C* 88 (6) (2013) 064002. arXiv:1310.2536, doi:10.1103/PhysRevC.88.064002.
- [4] R. Navarro Perez, J. Amaro, E. R. Arriola, Coarse grained NN potential with Chiral Two Pion Exchange, *Phys.Rev. C* 89 (2014) 024004. arXiv:1310.6972, doi:10.1103/PhysRevC.89.024004.
- [5] R. Navarro Perez, J. Amaro, E. Ruiz Arriola, Statistical Error analysis of Nucleon-Nucleon phenomenological potentials, *Phys.Rev. C* 89 (2014) 064006. arXiv:1404.0314, doi:10.1103/PhysRevC.89.064006.
- [6] R. B. Wiringa, V. Stoks, R. Schiavilla, An Accurate nucleon-nucleon potential with charge independence breaking, *Phys.Rev. C* 51 (1995) 38–51. arXiv:nuc1-th/9408016, doi:10.1103/PhysRevC.51.38.
- [7] V. Kukulin, M. Platonova, Short-range components of nuclear forces: Experiment versus mythology, *Phys.Atom.Nucl.* 76 (12) (2013) 1465–1481. doi:10.1134/S1063778813120120.
- [8] S. C. Pieper, R. B. Wiringa, Quantum Monte Carlo calculations of light nuclei, *Ann.Rev.Nucl.Part.Sci.* 51 (2001) 53–90. arXiv:nuc1-th/0103005, doi:10.1146/annurev.nucl.51.101701.132506.
- [9] J. Goldstone, Derivation of the Brueckner Many-Body Theory, *Proc.Roy.Soc.Lond.A Math.Phys.Eng.Sci.* 239 (1957) 267–279. doi:10.1098/rspa.1957.0037.
- [10] M. Moshinsky, Short range forces and nuclear shell theory, *Nuclear Physics* 8 (1958) 19 – 40.
- [11] T. Skyrme, The effective nuclear potential, *Nucl. Phys.* 9 (1959) 615–634.
- [12] S. A. Moszkowski, B. L. Scott, Nuclear forces and the properties of nuclear matter, *Annals of Physics* 11 (1960) 65–115. doi:10.1016/0003-4916(60)90128-7.
- [13] D. Vautherin, D. M. Brink, Hartree-Fock calculations with Skyrme’s interaction. 1. Spherical nuclei, *Phys. Rev. C* 5 (1972) 626–647. doi:10.1103/PhysRevC.5.626.
- [14] M. Bender, P.-H. Heenen, P.-G. Reinhard, Self-consistent mean-field models for nuclear structure, *Rev. Mod. Phys.* 75 (2003) 121–180. doi:10.1103/RevModPhys.75.121.
- [15] M. Dutra, O. Lourenco, J. Sa Martins, A. Delfino, J. Stone, et al., Skyrme Interaction and Nuclear Matter Constraints, *Phys.Rev. C* 85 (2012) 035201. arXiv:1202.3902, doi:10.1103/PhysRevC.85.035201.
- [16] E. R. Arriola, Low scale saturation of Effective NN Interactions and their Symmetries arXiv:1009.4161.
- [17] K. Harada, K. Inoue, H. Kubo, Wilsonian RG and redundant operators in nonrelativistic effective field theory, *Phys.Lett. B* 636 (2006) 305–309. arXiv:nuc1-th/0511020, doi:10.1016/j.physletb.2006.03.072.
- [18] R. Navarro Perez, J. Amaro, E. Ruiz Arriola, Effective Interactions in the Delta-Shells Potential, *Few Body Syst.* 54 (2013) 1487–1490. doi:10.1007/s00601-012-0537-5.

- [19] R. N. Perez, J. Amaro, E. R. Arriola, Error analysis of nuclear forces and effective interactions, J. Phys. G (in press), [arXiv:1406.0625](#).
- [20] S. K. Bogner, T. T. S. Kuo, A. Schwenk, D. R. Entem, R. Machleidt, Towards a unique low momentum nucleon nucleon interaction, Phys. Lett. B576 (2003) 265–272. [arXiv:nuc1-th/0108041](#), doi:10.1016/j.physletb.2003.10.012.
- [21] S. K. Bogner, T. T. S. Kuo, A. Schwenk, Model-independent low momentum nucleon interaction from phase shift equivalence, Phys. Rept. 386 (2003) 1–27. [arXiv:nuc1-th/0305035](#), doi:10.1016/j.physrep.2003.07.001.
- [22] S. K. Bogner, R. J. Furnstahl, R. J. Perry, Similarity Renormalization Group for Nucleon-Nucleon Interactions, Phys. Rev. C75 (2007) 061001. [arXiv:nuc1-th/0611045](#), doi:10.1103/PhysRevC.75.061001.
- [23] S. K. Bogner, R. J. Furnstahl, S. Ramanan, A. Schwenk, Low-momentum interactions with smooth cutoffs, Nucl. Phys. A784 (2007) 79–103. [arXiv:nuc1-th/0609003](#), doi:10.1016/j.nuclphysa.2006.11.123.
- [24] L. Coraggio, A. Covello, A. Gargano, N. Itaco, T. T. S. Kuo, Shell-model calculations and realistic effective interactions, Prog. Part. Nucl. Phys. 62 (2009) 135–182. [arXiv:0809.2144](#), doi:10.1016/j.ppnp.2008.06.001.
- [25] S. K. Bogner, R. J. Furnstahl, A. Schwenk, From low-momentum interactions to nuclear structure, Prog. Part. Nucl. Phys. 65 (2010) 94–147. [arXiv:0912.3688](#), doi:10.1016/j.ppnp.2010.03.001.
- [26] R. Furnstahl, The Renormalization Group in Nuclear Physics, Nucl.Phys.Proc.Suppl. 228 (2012) 139–175. [arXiv:1203.1779](#), doi:10.1016/j.nuclphysbps.2012.06.005.
- [27] R. Furnstahl, K. Hebeler, New applications of renormalization group methods in nuclear physics, Rept.Prog.Phys. 76 (2013) 126301. [arXiv:1305.3800](#), doi:10.1088/0034-4885/76/12/126301.
- [28] J. D. Holt, T. T. S. Kuo, G. E. Brown, S. K. Bogner, Counter Terms for Low Momentum Nucleon-Nucleon Interactions, Nucl. Phys. A733 (2004) 153–165. [arXiv:nuc1-th/0308036](#), doi:10.1016/j.nuclphysa.2003.12.004.
- [29] E. Jurgenson, P. Navratil, R. Furnstahl, Evolving Nuclear Many-Body Forces with the Similarity Renormalization Group, Phys.Rev. C83 (2011) 034301. [arXiv:1011.4085](#), doi:10.1103/PhysRevC.83.034301.
- [30] R. Roth, A. Calci, J. Langhammer, S. Binder, Evolved Chiral NN+3N Hamiltonians for Ab Initio Nuclear Structure Calculations [arXiv:1311.3563](#).
- [31] M. H. Partovi, E. L. Lomon, Field theoretical nucleon-nucleon potential, Phys.Rev. D2 (1970) 1999–2032. doi:10.1103/PhysRevD.2.1999.
- [32] R. Machleidt, The Meson theory of nuclear forces and nuclear structure, Adv.Nucl.Phys. 19 (1989) 189–376.
- [33] A. Calle Cordon, E. Ruiz Arriola, Renormalization vs Strong Form Factors for One Boson Exchange Potentials, Phys. Rev. C81 (2010) 044002. [arXiv:0905.4933](#), doi:10.1103/PhysRevC.81.044002.
- [34] R. J. Furnstahl, Similarity Renormalization Group for Few-Body Systems, Few Body Syst. 44 (2008) 133–136. [arXiv:0711.3846](#), doi:10.1007/s00601-008-0274-y.
- [35] E. Anderson, et al., Block Diagonalization using SRG Flow Equations, Phys. Rev. C77 (2008) 037001. [arXiv:0801.1098](#), doi:10.1103/PhysRevC.77.037001.
- [36] K. Hebeler, Momentum space evolution of chiral three-nucleon forces, Phys.Rev. C85 (2012) 021002. [arXiv:1201.0169](#), doi:10.1103/PhysRevC.85.021002.
- [37] E. D. Jurgenson, P. Navratil, R. J. Furnstahl, Evolution of Nuclear Many-Body Forces with the Similarity Renormalization Group, Phys. Rev. Lett. 103 (2009) 082501. [arXiv:0905.1873](#), doi:10.1103/PhysRevLett.103.082501.
- [38] K. Tsukiyama, S. Bogner, A. Schwenk, In-Medium Similarity Renormalization Group for Nuclei, Phys.Rev.Lett. 106 (2011) 222502. [arXiv:1006.3639](#), doi:10.1103/PhysRevLett.106.222502.
- [39] K. D. Launey, T. Dytrych, J. P. Draayer, Similarity renormalization group and many-body effects in multiparticle systems, Phys.Rev. C85 (2012) 044003. doi:10.1103/PhysRevC.85.044003.
- [40] H. Hergert, S. Bogner, S. Binder, A. Calci, J. Langhammer, et al., In-Medium Similarity Renormalization Group with Chiral Two- Plus Three-Nucleon Interactions, Phys.Rev. C87 (3) (2013) 034307. [arXiv:1212.1190](#), doi:10.1103/PhysRevC.87.034307.
- [41] K. Tsukiyama, S. Bogner, A. Schwenk, In-Medium Similarity Renormalization Group for Open-Shell Nuclei, Phys.Rev. C85 (2012) 061304. [arXiv:1203.2515](#), doi:10.1103/PhysRevC.85.061304.
- [42] V. Timoteo, S. Szpigel, E. Ruiz Arriola, Symmetries of the Similarity Renormalization Group for Nuclear Forces, Phys.Rev. C86 (2012) 034002. [arXiv:1108.1162](#), doi:10.1103/PhysRevC.86.034002.
- [43] K. Launey, T. Dytrych, J. Draayer, Importance of symmetries in the similarity renormalization group approach, Bulg.J.Phys. 39 (2012) 271–281.
- [44] E. Ruiz Arriola, V. Timoteo, S. Szpigel, Nuclear Symmetries of the similarity renormalization group for nuclear forces, PoS CD12 (2013) 106. [arXiv:1302.3978](#).
- [45] S. K. Bogner, R. J. Furnstahl, R. J. Perry, Three-Body Forces Produced by a Similarity Renormalization Group Transformation in a Simple Model, Annals Phys. 323 (2008) 1478–1501. [arXiv:0708.1602](#), doi:10.1016/j.aop.2007.09.001.
- [46] E. D. Jurgenson, R. J. Furnstahl, Similarity Renormalization Group Evolution of Many-Body Forces in a One-Dimensional Model, Nucl. Phys. A818 (2009) 152–173. [arXiv:0809.4199](#), doi:10.1016/j.nuclphysa.2008.12.007.
- [47] S. Szpigel, R. J. Perry, Simple Applications of Effective Field Theory and Similarity Renormalization Group Methods [arXiv:nuc1-th/9906031](#).
- [48] E. Ruiz Arriola, S. Szpigel, V. Timoteo, Fixed points of the Similarity Renormalization Group and the Nuclear Many-Body Problem, Few Body Syst. 55 (2014) 971–975. [arXiv:1310.8246](#), doi:10.1007/s00601-014-0858-7.
- [49] E. Ruiz Arriola, S. Szpigel, V. S. Timoteo, Implicit Versus Explicit Renormalization of the NN Force: An S-Wave Toy Model, Few Body Syst. 55 (2014) 989–992. [arXiv:1310.8526](#), doi:10.1007/s00601-014-0811-9.
- [50] D. R. Entem, E. Ruiz Arriola, M. Pavon Valderrama, R. Machleidt, Renormalization of chiral two-pion exchange NN interactions. Momentum vs. coordinate space, Phys. Rev. C77 (2008) 044006. [arXiv:0709.2770](#), doi:10.1103/PhysRevC.77.044006.
- [51] S. Szpigel, V. S. Timoteo, F. d. O. Duraes, Similarity Renormalization Group Evolution of Chiral Effective Nucleon-Nucleon Potentials in the Subtracted Kernel Method Approach, Annals Phys. 326 (2011) 364–405. [arXiv:1003.4663](#), doi:10.1016/j.aop.2010.11.007.
- [52] J. V. Steele, R. Furnstahl, Regularization methods for nucleon-nucleon effective field theory, Nucl.Phys. A637 (1998) 46–62. [arXiv:](#)

- nucl-th/9802069, doi:10.1016/S0375-9474(98)00219-X.
- [53] V. G. J. Stoks, R. A. M. Klomp, C. P. F. Terheggen, J. J. de Swart, Construction of high quality N N potential models, Phys. Rev. C49 (1994) 2950–2962. [arXiv:nucl-th/9406039](#), doi:10.1103/PhysRevC.49.2950.
  - [54] V. G. J. Stoks, R. A. M. Kompl, M. C. M. Rentmeester, J. J. de Swart, Partial wave analysis of all nucleon-nucleon scattering data below 350-MeV, Phys. Rev. C48 (1993) 792–815. doi:10.1103/PhysRevC.48.792.
  - [55] S. D. Glazek, K. G. Wilson, Renormalization of Hamiltonians, Phys. Rev. D48 (1993) 5863–5872. doi:10.1103/PhysRevD.48.5863.
  - [56] S. D. Glazek, K. G. Wilson, Perturbative renormalization group for Hamiltonians, Phys. Rev. D49 (1994) 4214–4218. doi:10.1103/PhysRevD.49.4214.
  - [57] F. J. Wegner, Flow equations for hamiltonians, Physics Reports 348 (1-2) (2001) 77 – 89.
  - [58] S. Kehrein, The flow equation approach to many-particle systems, Springer, 2006.
  - [59] E. Ruiz Arriola, S. Szpigel, V. Timoteo, The infrared limit of the Similarity Renormalization Group evolution and Levinson’s theorem, Phys.Lett. B735 (2014) 149–156. [arXiv:1404.4940](#), doi:10.1016/j.physletb.2014.06.032.
  - [60] J. W. Holt, G. E. Brown, Separation of Scales in the More Effective Field Theory and Moszkowski-Scott Methods [arXiv:nucl-th/0408047](#).
  - [61] E. Ruiz Arriola, Van der Waals forces and Photon-less Effective Field Theories, Few Body Syst. 50 (2011) 399–402. [arXiv:1012.2284](#), doi:10.1007/s00601-010-0203-8.

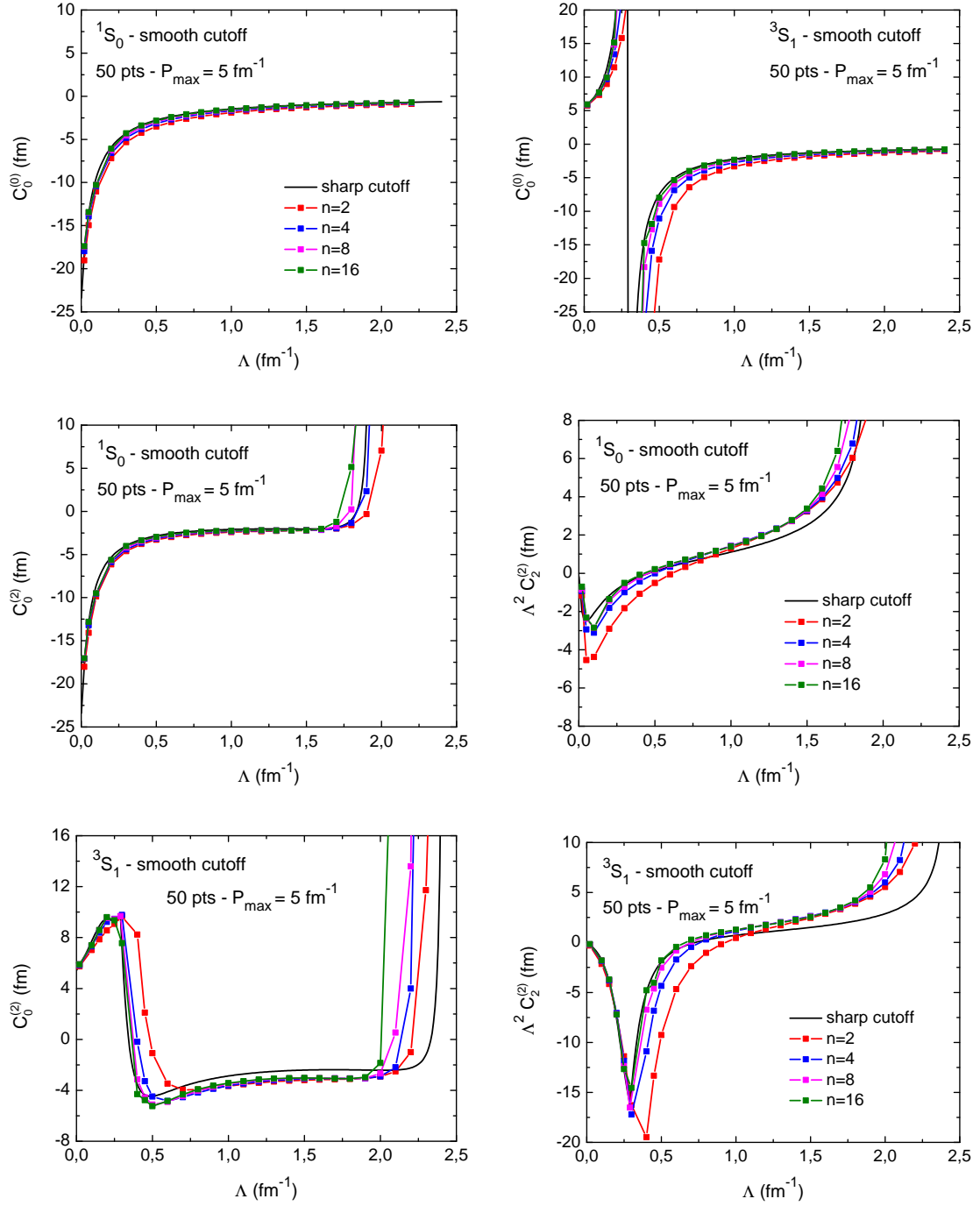


Figure 3: Running of the strength  $C_0^{(0)}$  with the cutoff  $\Lambda$  for the contact theory on a finite momentum grid regulated by a smooth cutoff for the  $^1S_0$  and  $^3S_1$  channels at LO (upper panels) and at NLO (middle panels:  $^1S_0$ , lower panels:  $^3S_1$ ). For comparison, we also show the corresponding  $C_0^{(0)}$  for the contact theory in the continuum regulated by a sharp momentum cutoff. In both cases the strengths are determined from the solution of the  $LS$  equation for the on-shell  $K$ -matrix by fitting the ERE parameters.



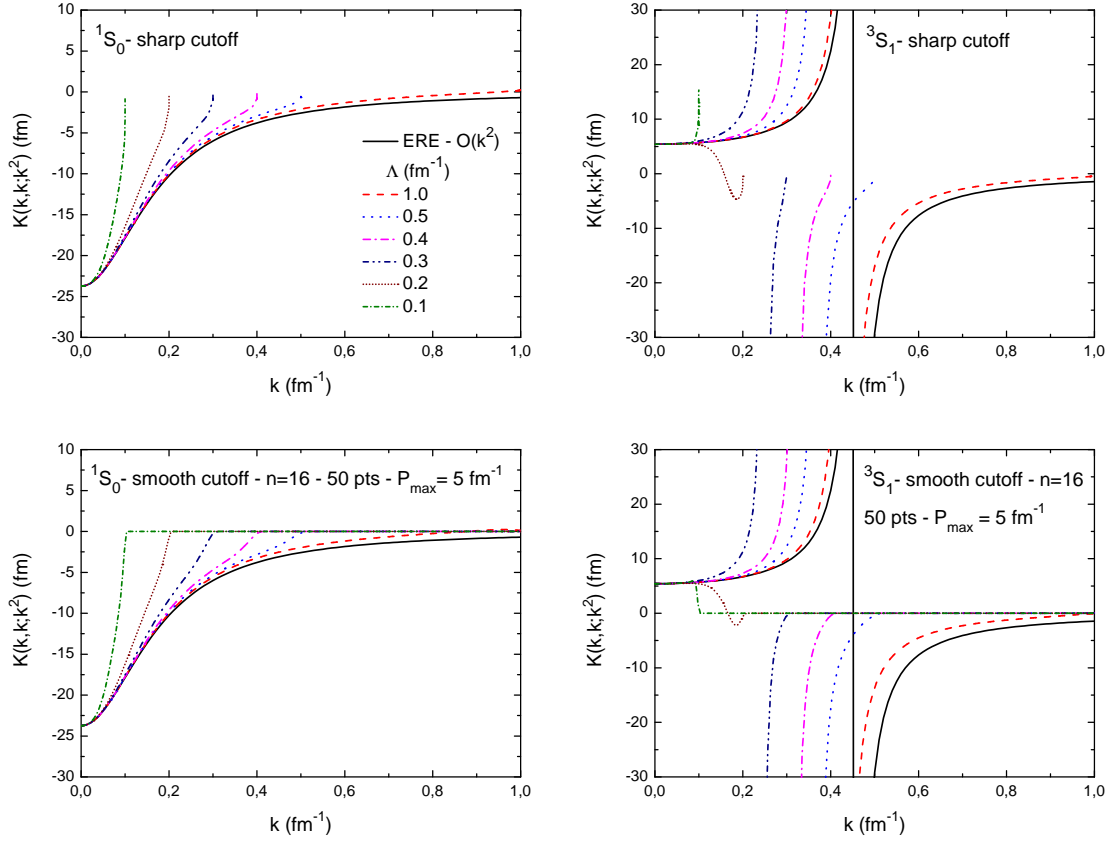


Figure 4: On-shell  $K$ -matrix for the  $^1S_0$  channel and the  $^3S_1$  channel  $NN$  potentials at  $NLO$ . Top panels: contact theory in the continuum regulated by a sharp momentum cutoff; Bottom panels: contact theory on a finite momentum grid with  $N = 50$  points regulated by a smooth exponential momentum cutoff. For comparison, we also show the on-shell  $K$ -matrix in the ERE to order  $O(k^2)$ .

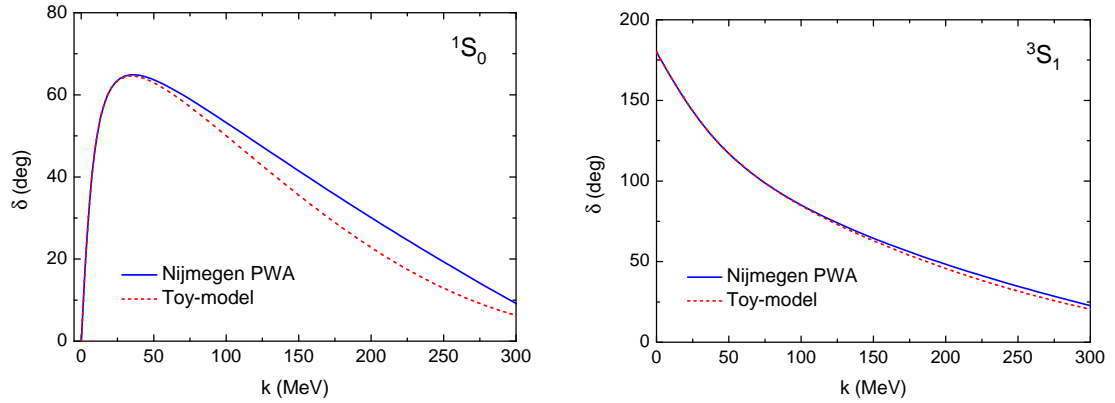


Figure 5:  $^1S_0$  and  $^3S_1$  phase-shifts for the toy-model separable gaussian potential compared to the results from the Nijmegen PWA [54].

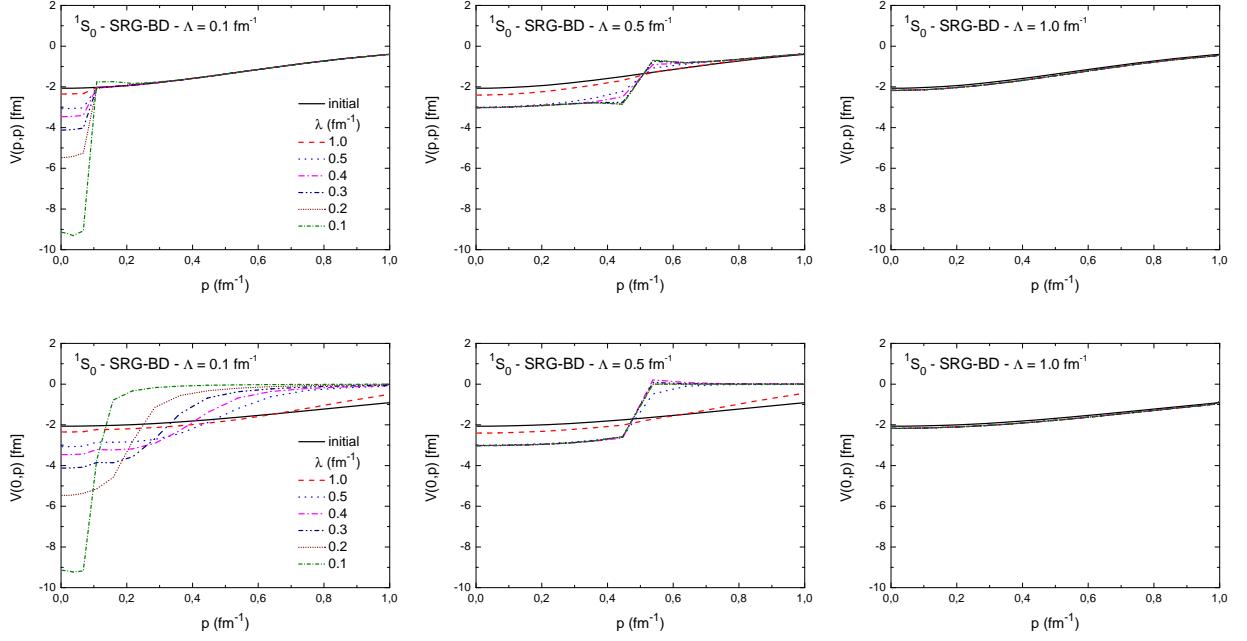


Figure 6: Diagonal (upper panels) and fully off-diagonal (lower panels) matrix-elements for the  $^1S_0$  channel toy-model potential on a gaussian grid (with  $N = 50$  momentum points and  $P_{\max} = 5 \text{ fm}^{-1}$ ) evolved through the SRG transformation with the block-diagonal generator to different SRG cutoffs  $\lambda$  for some values of the block-diagonal cutoff  $\Lambda$ . For comparison, we also show the diagonal matrix-elements for the initial ( $\lambda \rightarrow \infty$ ) toy-model potential.

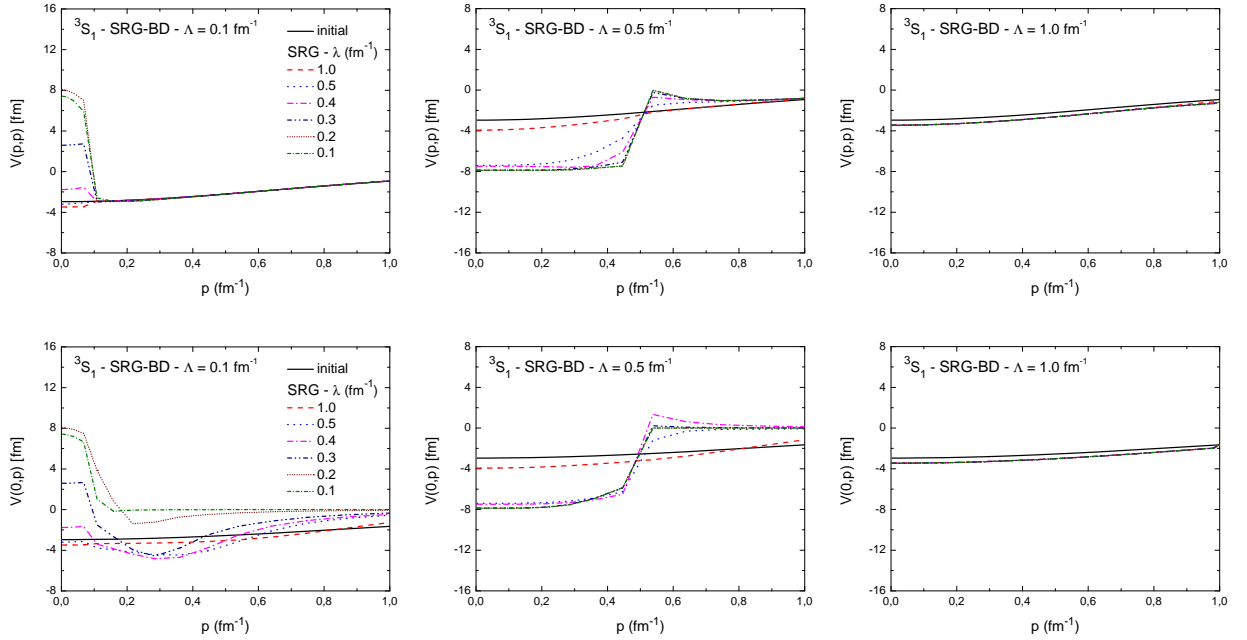


Figure 7: Diagonal (upper panels) and fully off-diagonal (lower panels) matrix-elements for the  $^3S_1$  channel toy-model potential on a gaussian grid (with  $N = 50$  momentum points and  $P_{\max} = 5 \text{ fm}^{-1}$ ) evolved through the SRG transformation with the block-diagonal generator to different SRG cutoffs  $\lambda$  for some values of the block-diagonal cutoff  $\Lambda$ . For comparison, we also show the diagonal matrix-elements for the initial ( $\lambda \rightarrow \infty$ ) toy-model potential.

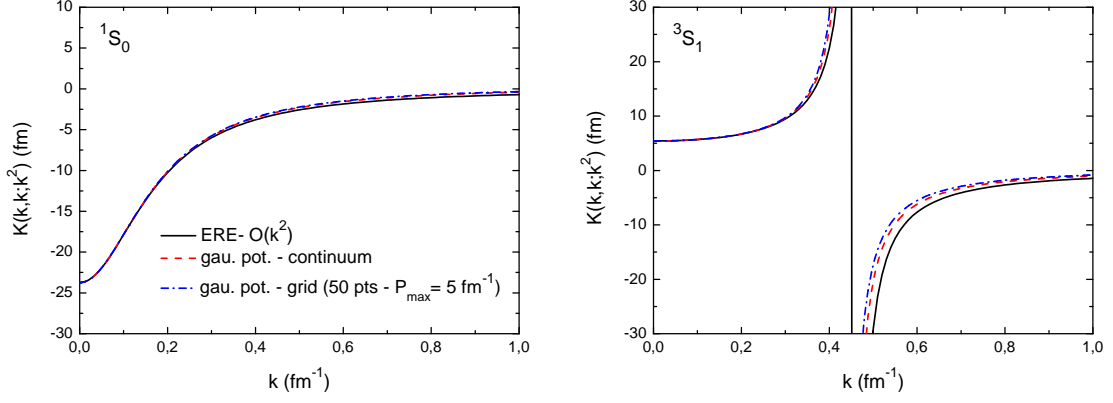


Figure 8: On-shell  $K$ -matrices for the  $^1S_0$  channel and the  $^3S_1$  channel toy-model potentials in the continuum and on a gaussian grid (with  $N = 50$  momentum points and  $P_{\max} = 5 \text{ fm}^{-1}$ ). For comparison, we also show the on-shell  $K$ -matrices in the ERE to order  $O(k^2)$ .

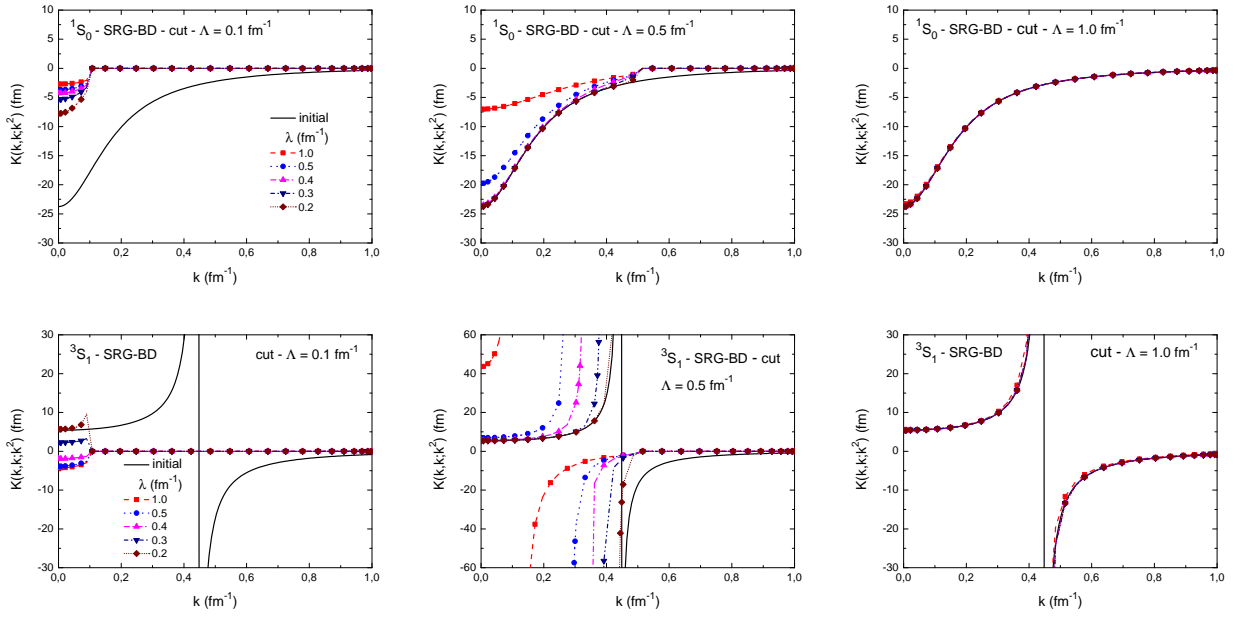


Figure 9: On-shell  $K$ -matrices for the  $^1S_0$  (upper panels) and  $^3S_1$  (lower panels) channels SRG-evolved toy-model potentials cut at the block-diagonal cutoff  $\Lambda$  (i. e. with the matrix-elements set to zero for momenta above  $\Lambda$ ). For comparison, we also show the on-shell  $K$ -matrix for the initial ( $\lambda \rightarrow \infty$ ) toy-model potential.

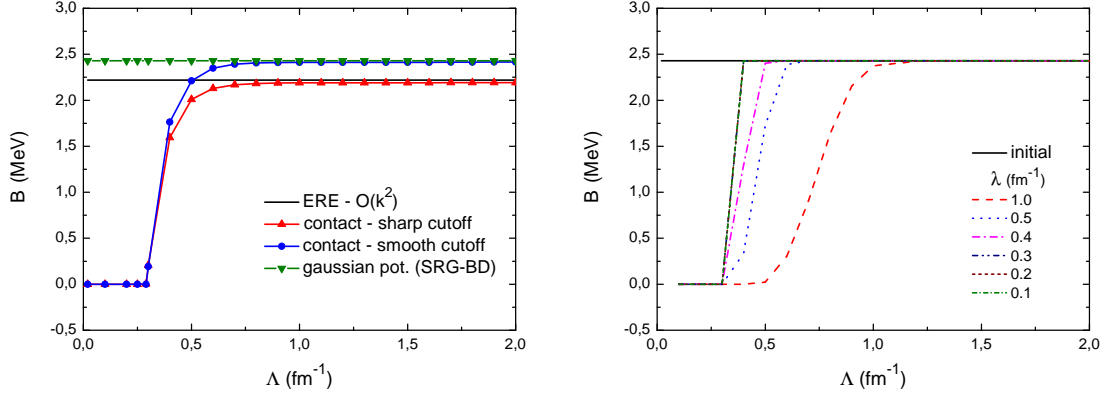


Figure 10: Left: deuteron binding-energy as a function of the cutoff scale  $\Lambda$  evaluated from the numerical solution of Schrödinger's equation with the  ${}^3S_1$  channel potential at  $NLO$  for the contact theory in the continuum with a sharp cutoff and for the contact theory on a gaussian grid with a smooth cutoff (with  $N = 50$  momentum points,  $P_{\text{max}} = 5 \text{ fm}^{-1}$  and  $n = 16$ ). For comparison, we also show the binding-energy obtained for the toy-model potential and the binding-energy obtained from the ERE to order  $\mathcal{O}(k^2)$ . Right: Deuteron binding-energy as a function of the block-diagonal cutoff  $\Lambda$  evaluated from the numerical solution of Schrödinger's equation with the SRG-evolved toy-model potential in the  ${}^3S_1$  channel cut at  $\Lambda$  (i.e. with the matrix-elements set to zero for momenta above  $\Lambda$ ). For comparison, we also show the binding-energy for the initial ( $\lambda \rightarrow \infty$ ) toy-model potential.

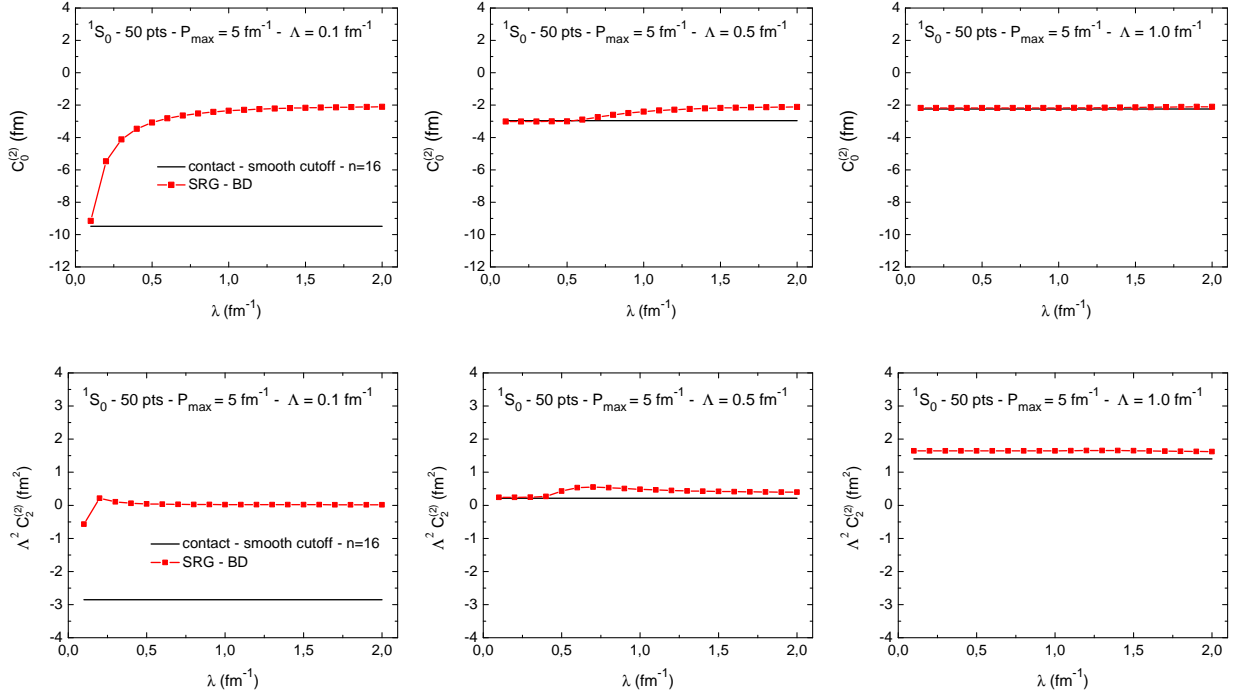


Figure 11:  $\tilde{C}_0^{(2)}$  (upper panels) and  $\tilde{C}_2^{(2)}$  (lower panels) as a function of the SRG cutoff  $\lambda$  extracted from the  ${}^1S_0$  channel toy-model potential on a gaussian grid (with  $N = 50$  momentum points and  $P_{\text{max}} = 5 \text{ fm}^{-1}$ ) evolved through the SRG transformation with the block-diagonal generator for some values of the block-diagonal cutoff  $\Lambda$ . For comparison, we also show  $C_0^{(2)}$  for the  ${}^1S_0$  channel contact theory potential at  $NLO$  (on the same grid) regulated by a smooth exponential momentum cutoff with  $n = 16$ .

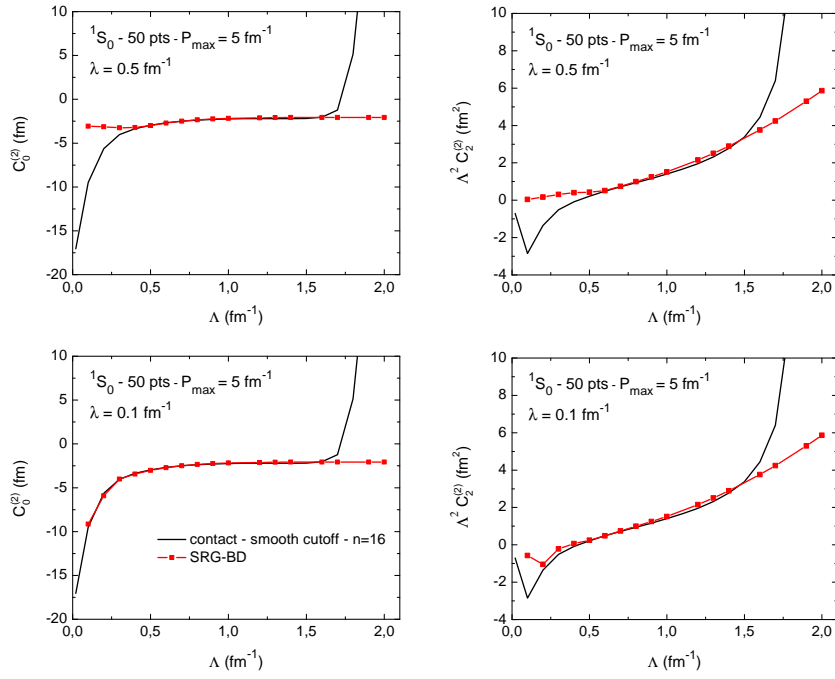


Figure 12:  $\tilde{C}_0^{(2)}$  and  $\tilde{C}_2^{(2)}$  as a function of the block-diagonal cutoff  $\Lambda$  extracted from the  $^1S_0$  channel toy-model potential on a gaussian grid (with  $N = 50$  momentum points and  $P_{\text{max}} = 5 \text{ fm}^{-1}$ ) evolved through the SRG transformation with the block-diagonal generator for two values of the SRG cutoff  $\lambda$ . For comparison, we also show  $C_0^{(2)}$  and  $C_2^{(2)}$  for the  $^1S_0$  channel contact theory potential at  $NLO$  (on the same grid) regulated by a smooth exponential momentum cutoff with  $n = 16$ .

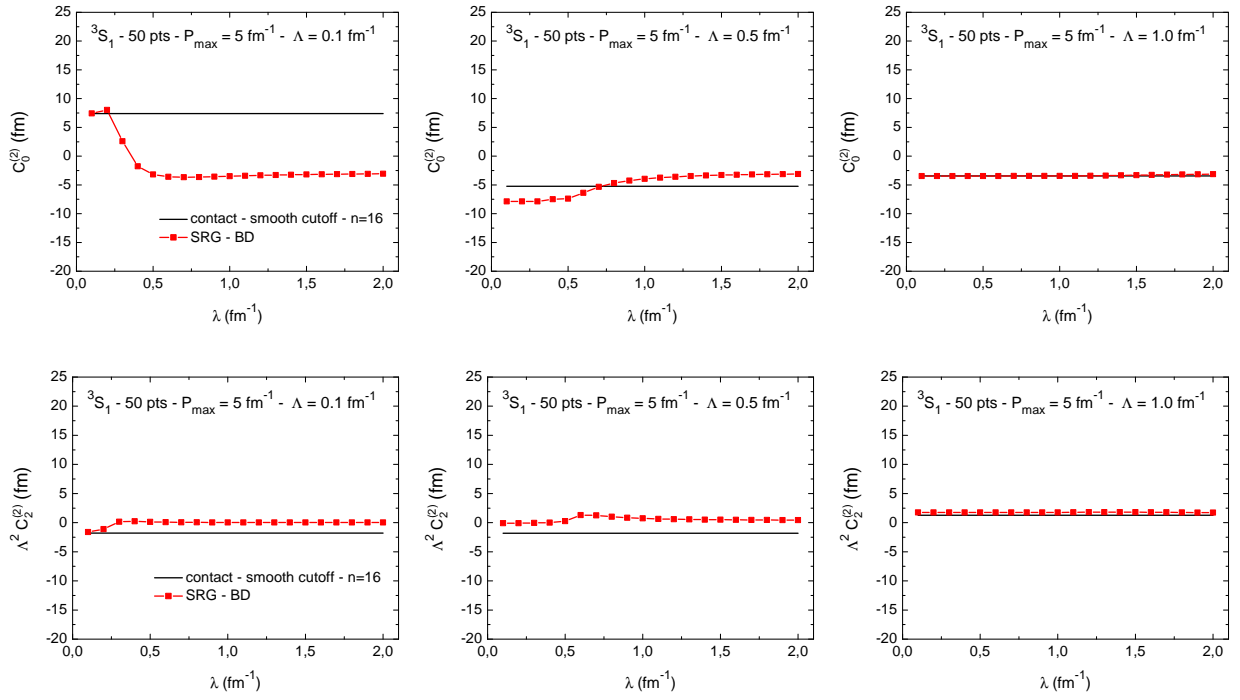


Figure 13:  $\tilde{C}_0^{(2)}$  as a function of the SRG cutoff  $\lambda$  extracted from the  $^3S_1$  channel toy-model potential on a gaussian grid (with  $N = 50$  momentum points and  $P_{\text{max}} = 5 \text{ fm}^{-1}$ ) evolved through the SRG transformation with the block-diagonal generator for some values of the block-diagonal cutoff  $\Lambda$ . For comparison, we also show  $C_0^{(2)}$  for the  $^3S_1$  channel contact theory potential at  $NLO$  (on the same grid) regulated by a smooth exponential momentum cutoff with  $n = 16$ .

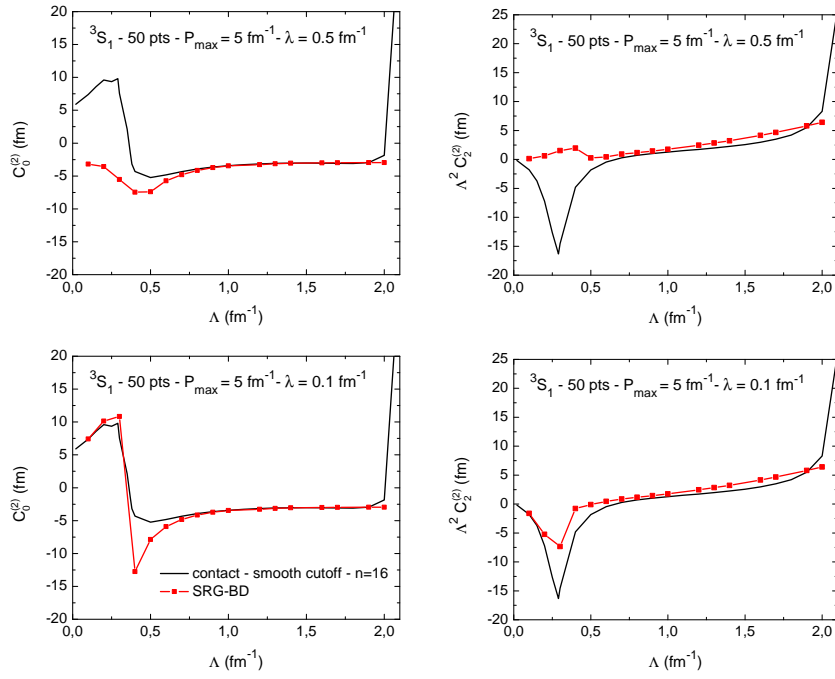


Figure 14:  $\tilde{C}_0^{(2)}$  and  $\tilde{C}_2^{(2)}$  as a function of the block-diagonal cutoff  $\Lambda$  extracted from the  $^3S_1$  channel toy-model potential on a gaussian grid (with  $N = 50$  momentum points and  $P_{\text{max}} = 5 \text{ fm}^{-1}$ ) evolved through the SRG transformation with the block-diagonal generator for several values of the SRG cutoff  $\lambda$ . For comparison, we also show  $C_0^{(2)}$  and  $C_2^{(2)}$  for the  $^3S_1$  channel contact theory potential at  $NLO$  (on the same grid) regulated by a smooth exponential momentum cutoff with  $n = 16$ .